

Responses to Referee #1

Thank you very much for your kind and constructive suggestions in such detail. And we deeply appreciate your fairly good patience, the time and energy devoted for reviewing our manuscript. We have modified the manuscript following your kind comments one by one.

Q1: A general effort of editing should be carried out to clarify some passages and improve the readability of the manuscript. On the enclosed copy, I marked statements that need to be corrected and/or rephrased, reporting some suggestions, for which, however, the authors should verify that correctly reflect what they meant.

R1: We have modified the manuscript following your kind comments one by one, see Line 16, 43, 48, 79-84, 85, 142-146, 150-151, 156-160, 170, 182, 186-189, 194-195, 196-198, 205-207, 219, 222, 255, 267, 279, 303, 310-311, 311-313, 313-316, 316-317, 473, 500, 526 and 555 in the revision.

Q2: The geological setting of the study area seems to be too poorly illustrated: an at least schematic map of the study area geology should be provided.

R2: Yes, we have added a geologic map of the study area showing lithology and faults, see Line 84 and 558 in the revision.

Q3: With regard to the statements of lines 156-159, it is unclear to me why an angle of $45^\circ + 1/2$ of friction angle was assumed as representative of sliding surface inclination on slopes where DEM provides angle greater than 60° . Clarification would be desirable.

R3: According to Jibson et al. (1998, 2000), slopes steeper than 60° remain unstable even at high strengths. We assume that Newmark's rigid plastic block is unsuitable for such a steep sliding surface. In this case, sliding occurs along a plane at an angle (α) of $45^\circ + \frac{\phi_b}{2}$ of the friction angle with the horizon. Therefore, we assigned an angle (α) of $45^\circ + \frac{\phi_b}{2}$ to slopes steeper than 60° to avoid too small a value of F_s in the Newmark analysis. We have added a figure to make it clear, see Line 156-160 and 578 in the revision.

Q4: At lines 197-199, the authors declare that the critical acceleration was found to reach, in the study area, a maximum of 14 g in areas of lower susceptibility. This maximum seems to me meaningless for the context of a dynamic slope stability analysis. It could be reported that the areas with lower susceptibility are those with critical acceleration greater than 1 g.

R4: Changes were made in the revision, see Line 196-198 in the revision.

Q5: At lines 262-263, the authors state that “most of the actual triggered landslides lie in the higher confidence-level areas with CF values greater than 0.60”. It would be desirable to have a more quantitative information at this regard: what is the percentage of such landslides?

R5: The quantitative portion of the actual triggered landslides lie in the higher confidence-level areas with CF values greater than 0.60 is 73.2%. Changes were made in the revision, see Line 260-261 in the revision.

Q6: In my opinion, Fig. 15 is poorly significant. The certainty factor CF and the proportion $p(H/E)$ occupied by landslides within areas falling in Newmark Displacement bins are two quantities uniquely related to each other, once the “a priori” probability $p(H)$ is fixed, through the equations (9) and the corresponding inverse functions reported on Fig. 15. Thus, the perfect fitting of black dots along the red curve depends merely by the fact that the black dots are randomly selected samples of the red curve itself. More significant would be to show how CF values are related to the Newmark Displacement values D_n , as Jibson et al. (2000) did for the proportion of landslide cells, corresponding to what is here defined $p(H/E)$, plotted versus D_n . In that study, it was this relation that was modelled through a Weibull curve, whose coefficients were derived by regression (see Fig. 14 of the cited paper). A similar plotting of CF as function of D_n would make possible to evaluate the consistency between these two quantities. Thus, one could obtain hazard estimates also for a seismic scenario different from the one used in the present study, once, following the same procedure described here, the D_n values expected for the new scenario is calculated.

R6: We consider your suggestion seriously and modify the manuscript depicted as follows: (1) for the statistical significance of the function of CF and Newmark displacement., the predicted displacement cells were grouped into bins based on quantile statistics. The breakpoints were 0, 10, 30, 39, 46, 51, 55, 59, 63, and 122. In this way, the number of cells in each bin was equal.; (2) as CF values ranged from -1 to 1, and not from 0 to 1, the Weibull (1939) curve developed by Jaeger and Cook (1969) is unsuitable here. Therefore, we modified the functional form to $CF=2k[1-\exp(-aD^b)]-1$, where CF is the certainty factor, m is the maximum CF value represented by the data, D is predicated displacement, and a and b are regression constants. In each bin, the CF value of Newmark displacement was plotted as a dot. The regression curve based on data from the Ludian earthquake is $CF=1.837[1-\exp(-0.073D^{0.821})]-1$; (3) when the predicted displacement increased, the value of CF increased monotonically, meaning that the confidence level for slope failure grew and landslide would probably occur. Such a procedure is consistent with the interpretation of certainty factor theory. Therefore, we were able to obtain estimates of the hazard different from the one used in this study using the same procedure described here. Changes were made in the revision, see Line 281-299.

Responses to Referee #2

Thanks very much for your nice comment. And we deeply appreciate your time devoted by reviewing our manuscript. Your constructive comments are invaluable to the improvement of our manuscript. We have modified the manuscript following your comments one by one.

Q1: The English writing should be improved. We suggest to be polished by a native English speaker.

R1: Yes, we have polished the manuscript with the help of a native English speaker, changes were made in the revision.

Q2: The geological map of Ludian earthquake should be added in Fig.1 including tectonic setting and the distribution of the faults.

R2: Yes, we have added a geologic map of the study area showing the distribution of lithology and faults, see Line 84 and 558 in the revision.

Q3: About introducing the CF method, I suggest to fit the Weibull curve as Jibson et al. (2000).

R3: Yes, we modified the Weibull function form developed by Jaeger and Cook (1969) to $CF=2k[1-\exp(-aD^b)]-1$, where CF is the certainty factor, m is the maximum CF value represented by the data, D is predicated displacement, and a and b are regression constants. The CF value of Newmark displacement was plotted as a dot. The regression curve based on data from the Ludian earthquake is $CF=1.837[1-\exp(-0.073D^{0.821})]-1$. With this function, we were able to obtain estimates of the hazard different from the one used in this study using the same procedure described here. Changes were made in the revision, see Line 281-299.

1 **An improved method of Newmark analysis for mapping hazards of**
2 **co-seismic landslides**

3

4 **Mingdong Zang^{1,2,3}, Shengwen Qi^{1,2,3}, Yu Zou^{1,2,3}, Zhuping Sheng⁴, Blanca S. Zamora⁴**

5

6 ¹Key Laboratory of Shale Gas and Geoengineering, Institute of Geology and Geophysics, Chinese
7 Academy of Sciences, Beijing 100029, China

8 ²Institutions of Earth Science, Chinese Academy of Sciences, Beijing 100029, China

9 ³University of Chinese Academy of Sciences, Beijing 100029, China

10 ⁴Texas A&M AgriLife Research Center at El Paso, El Paso, Texas 79927, USA

11

12 *Correspondence to: Shengwen Qi (qishengwen@mail.iggcas.ac.cn)*

13

14

15 **Abstract.** Coseismic landslides can destroy buildings, dislocate roads, sever pipelines, and cause heavy
16 casualties. It is thus important but challenging to accurately map the hazards posed by coseismic
17 landslides. Newmark's method is widely applied to assess the permanent displacement along a potential
18 slide surface and model the coseismic response of slopes. This paper proposes an improved Newmark
19 analysis for mapping the hazards of coseismic landslides by considering the roughness and effect of size
20 of the potential slide surfaces. This method is verified by data from a case study on the 2014 M_w 6.1 (the
21 United States Geological Survey) Ludian earthquake in Yunnan Province of China. Permanent
22 displacements due to the earthquake ranged from 0 to 122 cm. The predicted displacements were
23 compared with a comprehensive inventory of landslides triggered by the Ludian earthquake to map the
24 spatial variation in the hazards of coseismic landslides using the certainty factor model. The confidence
25 levels of coseismic landslides indicated by the certainty factors ranged from -1 to 0.95. A hazard map of
26 the coseismic landslide was generated based on the spatial distribution of values of the certainty factor. A
27 regression curve relating the predicted displacement and the certainty factor was drawn, and can be
28 applied to predict the hazards of coseismic landslides for any seismic scenario of interest. The area under
29 the curve was used to compare the improved and the conventional Newmark analyses, and revealed the
30 improved performance of the former. This mapping procedure can be used to predict the hazards posed
31 by coseismic landslides, and provide guidelines for decisions regarding the development of infrastructure
32 and post-earthquake reconstruction.

33 *Keywords:* Coseismic landslide; Newmark's method; Barton model; Certainty factor; Hazard mapping

34

35 **1 Introduction**

36 Earthquakes are recognized as one of the major causes of landslides (Keefer, 1984). Hazards caused by
37 coseismic landslides have drawn increasing attention in recent years (e.g., Jibson et al., 1998, 2000;
38 Khazai and Sitar, 2004; Qi et al., 2010, 2011, 2012; Chen et al., 2012; Xu et al., 2013; Yuan et al., 2014).

39 The damage caused by seismically triggered landslides is sometimes more severe than the direct damage
40 caused by the earthquake (Keefer, 1984). Estimating where a specific shaking is likely to induce a slope
41 failure plays an important role in the regional assessment of coseismic landslides.

42 Pseudostatic analysis formalized by Terzaghi (1950), and finite-element modeling applied by Clough and
43 Chopra (1966) have been employed to assess the seismic stability of slopes in early efforts (Jibson, 2011).

44 Newmark (1965) first introduced a relatively simple and practical method, which is still commonly used

45 nowadays, to estimate the coseismic permanent displacements of slopes (Jibson, 2011). Studies have
46 shown that Newmark's method yields reasonable and practical results when modeling the dynamic

47 performance of natural slopes (Wilson and Keefer, 1983; Wieczorek et al., 1985; Jibson et al., 1998, 2000;

48 Pradel et al., 2005). Rathje and Antonakos (2011) recently presented a unified framework for predicting

49 coseismic permanent sliding displacement based on Newmark's method. Chen et al. (2018) used

50 Newmark's method to calculate the minimum accelerations required for coseismic landslides in the region

51 affected by the 2014 Ludian earthquake. Chen et al. (2019) subsequently developed an easy-operation

52 mapping method to assess hazards posed by coseismic landslides in the zone struck by the 2014 Ludian

53 earthquake using Newmark's method.

54 Such applications generally start from an analysis of the dynamic stability of slopes, which is quantified

55 as the critical acceleration. Barton model (Barton, 1973) has been widely used in rock mechanics and

56 engineering to predict the shear strength of rock joints, which plays a crucial role in the calculation of
57 critical acceleration. However, researchers have not adequately attended to the shear strength of rock
58 joints during the assessment of coseismic landslides. To better estimate the dynamic stability of slopes, in
59 this paper, we introduce the Barton model (Barton, 1973) to Newmark analysis to develop an improved
60 modeling method for mapping the hazards posed by coseismic landslides using data from the 2014 Ludian
61 earthquake in Yunnan Province in southwestern China. As predictions of coseismic landslides are not
62 based on exact results, i.e., the computed permanent displacements, but are also mingled with
63 unformalized expertise, i.e., the interpreted landslides, we present a model of inexact reasoning, i.e., the
64 certainty factor model (CFM), that defies analysis, as an application of sets of inference rules that are
65 expressed in predicate logic (Shortliffe and Buchanan, 1975), to produce a map of the hazards posed by
66 coseismic landslides.

67 This paper briefly introduces the characteristics and spatial distribution of landslides triggered at the
68 chosen site, describes the method of modeling used for the analysis of the stability of seismic slopes,
69 presents the mapping procedure of the confidence level of seismic slope failure, and finally discusses the
70 results of the assessment of seismic hazard as well as a comparison with the conventional Newmark
71 analysis.

72

73 **2 Study area**

74 The epicenter of the 2014 M_w 6.1 (the United States Geological Survey) Ludian earthquake was located
75 in the southeastern margin of the Tibetan Plateau. A rectangular area lying immediately around the
76 epicenter containing dense concentrations of the induced landslides was chosen for study (Fig. 1). The

77 elevation of the area ranged from 785 m to 3,085 m above sea level. Three rivers—the Niulanjiang River,
78 Shaba River, and Longquan River—pass through the study area (Fig. 1). The topography ranges from flat
79 in the river valleys to nearly vertical in the slopes on the banks of the rivers. According to Chen et al.
80 (2015), Niulanjiang River flows from the southeast (SE) to the northwest (NW), and incises to a depth
81 between 1,200 m and 3,300 m, resulting in about 80% of the slopes having angles greater than 40°
82 distributed along the banks. The predominant geological units of the study area have an age that varies
83 from the Proterozoic to the Mesozoic, including dolomite, limestone, shale, sandstone, basalt, and slate
84 (Fig. 2).

85 An inventory of 1,416 landslides triggered by the 2014 Ludian earthquake (Fig. 1) was compiled by visual
86 inspection through comparisons between pre-earthquake satellite images obtained from Google Earth
87 (January 30, 2014) and 0.2-m high-resolution post-earthquake aerial images (August 7, 2014; data
88 provided by the Digital Mountain and Remote Sensing Applications Center, Institute of Mountain
89 Hazards and Environment, Chinese Academy of Sciences, and Beijing Anxiang Power Technology Co.,
90 LTD.). A majority of landslides triggered by the earthquake were shallow, flow-like landslides (shallower
91 than 3 m), developing in particularly dense concentrations along steeply incised river valleys. The total
92 area of these interpreted landslides was 7.01 km² within a study area of 705 km². A detailed study showed
93 that 846 of the mapped landslides were greater than 1,000 m² in area, occupying 6.74 km² and accounting
94 for 96.1% of the total area of landslides, of which 279 were greater in area than 5,000 m², occupying 5.37
95 km² and accounting for 76.6% of the total landslide area.

96

97 **3 Methodology**

98 3.1 Modeling method

99 In the context of the analysis of the dynamic stability of a slope, Newmark (1965) proposed a permanent
100 displacement analysis that bridges the gap between simplistic pseudostatic analysis and sophisticated, but
101 generally impractical, finite element modeling (Jibson, 1993). Newmark's method simulates a landslide
102 as a rigid plastic friction block with a known critical acceleration on an inclined plane (Fig. 3), and
103 calculates the cumulative permanent displacement of the block as it is subjected to an acceleration-time
104 history of an earthquake. Newmark (1965) showed that the dynamic stability of a slope is related to the
105 critical acceleration of a potential landslide block, and can be expressed as a simple function of the static
106 factor of safety and the geometry of the landslide (Jibson et al., 1998, 2000):

$$a_c = (F_S - 1)g \sin \alpha \quad (1)$$

107 where a_c is the critical acceleration in terms of g , the acceleration due to the Earth's gravity, F_S is the
108 static factor of safety, and α is the angle from the horizontal at which the center of the slide block moves
109 when displacement first occurs (Jibson et al., 1998, 2000). For a planar slip surface parallel to the slope,
110 this angle generally approximates to the angle of the slope.

111 Natural slopes often develop a group of shallow unloading joints (Fig. 4) parallel to the surface due to
112 valley incisions (Gu, 1979; Hoek and Bray, 1981). Studies have shown that rock slopes behave as
113 collapsing and sliding failures of shallow unloading joints under strong earthquakes, and 90% of
114 coseismic landslides are shallow falls and slides (Harp and Jibson, 1996; Khazai and Sitar, 2003; Dai et
115 al., 2011; Tang et al., 2015). According to Qi et al. (2012), two typical kinds of landslides are triggered
116 by earthquakes, i.e., (a) shallow, flow-like landslides with depth less than 3 m in general, and (b) rock
117 falls thrown by the shaking caused by the earthquake, usually occurring at the crest of the slope. For both

118 types, **unstable blocks of rock** are often cut and activated along the rock joints. Therefore, the static factor
119 of safety in terms of the critical acceleration in these conditions is related to the peak shear strength of the
120 rock joints. For the purpose of **regional analysis**, we use a limit-equilibrium model of an infinite slope
121 (Fig. 3) by referring to the simplification of **Newmark's method** by of Jibson et al. (1998, 2000). The
122 value of the static factor of safety against sliding **given** by the ratio of **resistance** to **the** driving forces is
123 determined by conventional analysis **without considering** accelerations, expressed as:

$$F_s = \frac{\text{Resisting force}}{\text{Driving force}} = \frac{\tau L}{mgsin\alpha} = \frac{\tau L}{\gamma Ltsin\alpha} = \frac{\tau}{\gamma tsin\alpha} \quad (2)$$

124 where τ is **the** peak shear strength of the rock joint, **L is the length of the rock joint**, **m is the mass of**
125 **the failure rock block**, γ is **the** unit weight of the rock mass, and t is the thickness of the failure rock
126 block.

127 For a Newmark analysis, it **is** customary to describe the shear strength of rocks **instead of** rock joints in
128 terms of Coulomb's constants—friction angle (ϕ) and cohesion (c). However, both are not only stress
129 dependent, but also scale dependent (Barton and Choubey, 1977). According to Barton (1973), a more
130 satisfactory empirical relationship for predicting the peak shear strength of a joint can be written as
131 follows:

$$\tau = \sigma_n \tan [JRC \log_{10} \left(\frac{JCS}{\sigma_n} \right) + \phi_b] \quad (3)$$

132 where σ_n is **the** effective normal stress, **JRC is the joint roughness coefficient**, **JCS is the joint wall**
133 **compressive strength**, **and ϕ_b is the basic friction angle—the angle of frictional sliding resistance**
134 **between rock joints—which can be obtained from residual shear tests on natural joints (Barton, 1973).**

135 The effective normal stress (σ_n) generated by **gravity** acting on the rock block is as follows:

$$\sigma_n = \frac{mg\cos\alpha}{L} = \frac{\gamma L t \cos\alpha}{L} = \gamma t \cos\alpha \quad (4)$$

136 Considering the impact of **size on** JRC and JCS , **the formulations developed** by Barton and Bandis (1982)
 137 are shown as below:

$$JRC_n = JRC_0 \left(\frac{L_n}{L_0} \right)^{-0.02JRC_0} \quad (5)$$

$$JCS_n = JCS_0 \left(\frac{L_n}{L_0} \right)^{-0.03JRC_0} \quad (6)$$

138 where the nomenclature adopted **incorporates (0)** and (n) for **values of** the laboratory scale and **the** in-situ
 139 scale, respectively.

140 Hence, the static factor of safety (F_S) of a slope can be written as:

$$\begin{aligned} F_S &= \frac{\tau}{\gamma t \sin\alpha} = \frac{\sigma_n \tan [JRC_n \log_{10} \left(\frac{JCS_n}{\sigma_n} \right) + \phi_b]}{\gamma t \sin\alpha} \\ &= \frac{\gamma t \cos\alpha \tan [JRC_n \log_{10} \left(\frac{JCS_n}{\gamma t \cos\alpha} \right) + \phi_b]}{\gamma t \sin\alpha} \\ &= \frac{\tan [JRC_n \log_{10} \left(\frac{JCS_n}{\gamma t \cos\alpha} \right) + \phi_b]}{\tan\alpha} \end{aligned} \quad (7)$$

141 After **calculating the angle of the slope and static** factor of safety, the critical acceleration of **the** slope can
 142 be determined. Once the **time history of the earthquake' acceleration** has been selected, **portions** of the
 143 record lying above the critical acceleration a_c (Fig. 5a) are integrated once to derive a velocity profile

144 (Fig. 5b); the time history of velocity is then integrated a second time to obtain the profile of cumulative
145 displacement of the block (Fig. 5c). Users finally determine the dynamic performance of the slope based
146 on the magnitude of the Newmark displacement (Jibson et al., 1998, 2000; Jibson, 2011). The detailed
147 procedure of conducting a Newmark analysis with the Barton model is discussed in the following sections.

148 3.2 Static factor-of-safety map

149 Considering that the mapped landslides greater in area than 1,000 m² occupied 96.1% of the total landslide
150 area, we selected a 30 m × 30 m digital elevation model (DEM) from the ASTER Global Digital Elevation
151 Model (<https://doi.org/10.5067/ASTER/ASTGTM.002>, last accessed July 16, 2018), which facilitated the
152 subsequent hazard analysis. A basic slope algorithm was applied to the DEM to produce a slope map (Fig.
153 6), where the slope was identified as the steepest downhill descent from a cell to its neighbors (Burrough
154 and McDonnell, 1998). The slopes ranged from greater than 60° along the banks of the Niulanjiang River,
155 Shaba River, and Longquan River, to less than 20° in low mountains and hills in the north and east.

156 According to Jibson et al. (1998, 2000), slopes steeper than 60° remain unstable even at high strengths.
157 We assume that Newmark's rigid plastic block is unsuitable for such a steep sliding surface. In this case,
158 sliding occurs along a plane at an angle (α) of $45^\circ + \frac{\phi_b}{2}$ with the horizon (Fig. 7). Therefore, we assigned
159 an angle (α) of $45^\circ + \frac{\phi_b}{2}$ to slopes steeper than 60° to avoid too small a value of F_S in the Newmark
160 analysis.

161 The digital geological map from the China Geological Survey (CGS) was rasterized at a 30-m grid spacing
162 to assign material properties throughout the study area. According to the literature, JRC_0 and JCS_0
163 depend strongly on lithology (Coulson, 1972; Barton and Choubey, 1977; Bandis et al., 1983; Bilgin and

164 Pasamehmetoglu, 1990; Priest, 1993; Singh et al., 2012; Alejano et al., 2012, 2014; Giusepone, 2014;
165 Yong et al., 2018). Representative values of γ , JRC_0 , JCS_0 , and ϕ_b assigned to each rock type exposed
166 in the study area were estimated using the test data listed in Table 1. The selected values were near the
167 middle of the ranges represented in the references. These JRC_0 and JCS_0 values were considered in a
168 laboratory scale for a length of 100 mm as L_0 . For each grid cell in the regional analysis, the length of
169 the engineering dimension, L_n , can generally be set as a 10-fold range of L_0 . This is because the value
170 of JRC_n/JRC_0 (JCS_n/JCS_0) is nearly constant when the value of L_n/L_0 is greater than 10 (Bandis et al.,
171 1981). The values of JRC_n and JCS_n , then, were calculated by inserting the values of JRC_0 and JCS_0 ,
172 and L_0 , and L_n into Eqs. (5) and (6), respectively. Figures 8 and 9 show the spatial distributions of JRC_n
173 and JCS_n , respectively. The basic-friction-angle (ϕ_b) map and unit-weight (γ) map are shown in Figs. 10
174 and 11, respectively.

175 For the sake of simplicity, the thickness of the modeled block t was taken to be 3 m, which reflected the
176 typical slope failures of the Ludian earthquake. The static factor-of-safety map was produced by
177 combining these data layers (α , JRC_n , JCS_n , ϕ_b , and γ) in Eq. (7). In the initial iteration of the
178 calculation, grid cells in steep areas with static factors of safety smaller than one indicated that the slopes
179 were statically unstable, but did not necessarily mean that they were moving under shaking induced by
180 the earthquake. In this condition, to avoid conservative results, we neither increased the strengths of the
181 rock types with statically unstable cells nor adjusted the strengths of other rock types to preserve the
182 differences in relative strength between them (as in Jibson et al., 1998, 2000). Instead, we assigned a
183 minimal static factor of safety of 1.01, merely above limit equilibrium (Jibson et al., 1998, 2000), to these
184 slopes to avoid a negative value of the critical acceleration a_c . According to Keefer (1984), most

185 landslides triggered by earthquakes occur with a slope of at least 5° . The static factors of safety resulting
186 from slopes of angles smaller than 5° were very high. These slopes were unlikely to fail under the Ludian
187 earthquake, and did not produce a statistically significant sample in the analysis. Therefore, slopes less
188 steep than 5° were not analyzed in the second iteration. After the adjustment, the static factors of safety
189 ranged from 1 to 17.4, as shown in Fig. 12.

190 3.3 Critical acceleration map

191 According to Newmark (1965), a pseudostatic analysis in terms of the static factor of safety and the slope
192 angle was employed to calculate the critical acceleration of a potential landslide. The map of critical
193 acceleration (Fig. 13) was generated by combining the static factor of safety and the slope angle in Eq.
194 (1). The critical accelerations were derived from the intrinsic properties of the slope (topography and
195 lithology), regardless of the given shaking. Therefore, the map of critical acceleration indicated the
196 susceptibility of coseismic landslides (Jibson et al., 1998, 2000). The calculated critical accelerations
197 ranged from nearly zero in areas that were more susceptible to coseismic landslides to greater than $1\ g$
198 in areas that were less susceptibility.

199 3.4 Shake map

200 There were 23 strong-motion stations within 100 km of the epicenter of the Ludian earthquake (Fig. 14).
201 Each station's record contained the three components of the peak ground acceleration (*PGA*), south–north
202 direction, east–west direction, and up–down direction, as listed in Table 2 (the dataset was provided by
203 the China Earthquake Data Center, <http://data.earthquake.cn>, last accessed June 16, 2016). We calculated
204 the average *PGA* of the two horizontal components of each strong-motion recording and plotted a
205 contour map (Fig. 15) using an inverse distance-weighted (IDW) interpolation algorithm. It determined

206 the cell values using a linearly weighted combination of a set of sample stations with weights inversely
207 proportional to distance (Watson and Philip, 1985). In addition, given that input stations far from the
208 epicenter, where the prediction was made, might have had poor or no spatial correlation, we eliminated
209 the input stations beyond 100 km from the epicenter from the calculation.

210 3.5 Newmark displacement map

211 In case of a landslide in practice, it is impossible to conduct a rigorous Newmark analysis when
212 accelerometer records are unavailable. It is also impractical and time consuming to produce a
213 displacement in each cell during the regional analysis. Therefore, empirical regressions (Ambraseys and
214 Menu, 1988; Bray and Travasarou, 2007; Jibson, 2007; Saygili and Rathje, 2008; Rathje and Saygili,
215 2009; Hsieh and Lee, 2011) have been proposed to estimate Newmark displacement as a function of the
216 critical acceleration and peak ground acceleration, or the Arias intensity. Rathje and Saygili (2009)
217 developed a vector model for displacement in terms of the critical acceleration (a_c), peak ground
218 acceleration (PGA), and moment magnitude (M_w) based on an analysis of over 2,000 strong motion
219 recordings:

$$\begin{aligned} \ln D = & 4.89 - 4.85 \left(\frac{a_c}{PGA} \right) - 19.64 \left(\frac{a_c}{PGA} \right)^2 + 42.49 \left(\frac{a_c}{PGA} \right)^3 - 29.06 \left(\frac{a_c}{PGA} \right)^4 \\ & + 0.72 \ln(PGA) + 0.89(M_w - 6) \end{aligned} \quad (8)$$

220 where D is the predicted displacement in units of cm , and a_c and PGA are in units of g .
221 This model is a preferred displacement model at a site where acceleration-time recordings are not
222 available. Incorporating multiple parameters of ground motion into the analysis typically results in less
223 variation in the prediction of displacement (Rathje and Saygili, 2009).

224 The Newmark displacement of each cell was calculated by combining the corresponding values of the
225 critical acceleration, peak ground acceleration, and moment magnitude in Eq. (8). The predicted
226 displacements ranged from 0 cm to 122 cm, as shown in Fig. 16.

227 3.6 Coseismic landslide hazard map

228 According to Jibson et al. (1998, 2000), predicted displacements provide an index of the seismic
229 performance of slopes, where larger predicted displacements relate to a greater incidence of slope failures.
230 But the displacements do not correspond directly to measurable slope movements in the field. To produce
231 a coseismic landslide hazard map, we chose a model of inexact reasoning, the certainty factor model
232 (CFM), created by Shortliffe and Buchanan (1975) and improved by Hecherman (1986), to explore the
233 relationship between the occurrences of landslides and their predicted displacements. The CFM was
234 created as a numerical method, initially used in MYCIN, a backward-chaining expert system in medicine
235 (Shortliffe and Buchanan, 1975), for managing uncertainty in a rule-based system. In this model, the
236 certainty factor CF represents the net confidence in a hypothesis H based on the evidence E
237 (Hecherman, 1986). Certainty factors range between -1 and 1. A CF with a value of -1 means a total lack
238 of confidence, whereas a CF with a value of 1 means total confidence. Values greater than zero favor
239 the hypothesis while those less than zero favor its negation. According to Hecherman (1986), the
240 probabilistic interpretation of CF is as follows:

$$CF = \begin{cases} \frac{p(H|E) - p(H)}{p(H|E)[1 - p(H)]}, & p(H|E) > p(H) \\ \frac{p(H|E) - p(H)}{p(H)[1 - p(H|E)]}, & p(H|E) < p(H) \end{cases} \quad (9)$$

241 where CF is the certainty factor, $p(H|E)$ denotes the conditional probability for a posterior hypothesis
242 that relies on evidence, the posterior probability, and $p(H)$ is the prior probability before any evidence
243 is known. In the displacement analysis, $p(H|E)$ was defined as the proportion of the area of the landslide
244 within a specific displacement area, and $p(H)$ was defined as the proportion of the landslide area within
245 the entire study area, excluding slopes less steep than 5° . In this way, the values of CF represented the
246 confidence level for coseismic landslides. Positive values corresponded to an increase in the confidence
247 level in slope failure while negative quantities corresponded to a decrease in this confidence. Higher
248 positive values indicated higher confidence levels for coseismic landslides.

249 Given the above definition, we produced a coseismic landslide hazard map in terms of the certainty factors.
250 First, displacement cells every 1 cm were grouped into bins such that all cells with displacements between
251 0 cm and 1 cm were grouped into the first bin, those with displacements between 1 cm and 2 cm were
252 grouped into the second bin, and so on. The displacements were grouped into 123 bins, from 0 cm to 122
253 cm. We then calculated the proportion of cells occupied by areas of landslides in each bin. This proportion
254 was considered the posterior probability of each bin as defined. The prior probability calculated by
255 dividing the entire landslide area by the entire study area was the same in each bin. Finally, the values of
256 CF were computed in each bin by using Eq. (9) to combine the corresponding values of the posterior and
257 prior probabilities. The certainty factors ranged from -1 to 0.95. The values of CF indicated the
258 confidence level of the occurrence of a landslide for each bin in the study area, and provided the basis for
259 producing the coseismic landslide hazard map.

260 As shown in the hazard map (Fig. 17), 73.2% of landslides triggered by the Ludian earthquake were in
261 areas with higher confidence levels, with CF values greater than 0.6. The interpreted landslides were

262 covered on the map to demonstrate **their goodness of fit** for **the** predicted confidence levels **for** coseismic
263 landslides (Fig. 17).

264

265 **4 Results and discussion**

266 The predicted displacements represent the cumulative sliding displacements for a given **time history of**
267 **acceleration**. Based on the statistically significant sizes of the **areas**, displacements less than 60 cm, which
268 **was** around the middle of **the range of displacement**, **occupied** about 80% of the study area **while**
269 displacements greater than 80 cm **occupied** a very small area. Jibson et al. (1998, 2000) **assumed** that
270 shallow falls and slides in brittle, weakly cemented materials **fail** at a relatively small displacement,
271 **whereas** slumps and block slides in more compliant materials **likely** fail at a larger displacement. That is
272 to say, the study area **was** more susceptible to rock falls and shallow, disrupted slides that fail at a relatively
273 small displacement. **By contrast, it was subjected with a lower probability** to coherent, deep-seated slides
274 that would fail at a larger displacement. Indeed, the majority of landslides triggered by the Ludian
275 earthquake were shallow, disrupted slides and rock falls (Zhou et al., 2016). Although **a few catastrophic**
276 rock avalanches, such as the Hongshiyan landslide (Chang et al., 2017), occurred in the field, they did not
277 produce statistically significant samples that could meaningfully contribute to the model, which **is**
278 consistent with the statistical results as discussed **above**. Therefore, the model should relate well to typical
279 kinds of earthquake-induced landslides in the study area, **thus demonstrating its usefulness in predicting**
280 the probability of other types of landslides.

281 **According to Jibson et al. (1998, 2000), a function of CF and Newmark displacement would make it**
282 **possible to predict the spatial variation in coseismic landslides in any scenario of interest involving the**

283 ground shaking. As mentioned above, 80% of the study area featured predicted displacements of less than
284 60 cm. The numbers of the Newmark displacement cells were uneven. There were more cells in 1 cm bins
285 for smaller displacements and fewer cells in 1 cm bins for larger ones. This might have affected the
286 statistical significance of the function of CF and Newmark displacement. Therefore, the predicted
287 displacement cells were grouped into bins based on quantile statistics. The breakpoints were 0, 10, 30, 39,
288 46, 51, 55, 59, 63, and 122. In this way, the number of cells in each bin was equal. Figure 18 shows, in
289 each bin, the CF value of the Newmark displacement as plotted as a dot. As CF values ranged from -1
290 to 1, and not from 0 to 1, the Weibull (1939) curve developed by Jaeger and Cook (1969) is unsuitable
291 here. Therefore, we modified the functional form as below:

$$CF = 2k[1 - \exp(-aD^b)] - 1 \quad (10)$$

292 where CF is the certainty factor, k is the maximum CF value represented by the data, D is predicted
293 displacement, and a and b are regression constants. The regression curve based on data from the
294 Ludian earthquake is

$$CF = 1.837[1 - \exp(-0.073D^{0.821})] - 1 \quad (11)$$

295 From the curve shown in Fig. 18, when the predicted displacement increased, the value of CF increased
296 monotonically, meaning that the confidence level for slope failure grew and landslide would probably
297 occur. Such a procedure is consistent with the interpretation of certainty factor theory. Therefore, we were
298 able to obtain estimates of the hazard different from the one used in this study using the same procedure
299 described here.

300 When fitting the results of shear tests using Coulomb's linear relation, the shear strengths varied widely
301 from high normal stress in the laboratory to low normal stress in the field (Barton, 1973). We introduced
302 the Barton model to the Newmark analysis to reduce the variation in shear strength in terms of Coulomb's
303 constants. We also considered the impact of scale effects by using Eqs. (5) and (6) to prevent Newmark's
304 method from underestimating the shear strength of geological units in regional analysis. In addition, for
305 the Barton model, the joint roughness coefficient (*JRC*) was estimated from tilt tests, or by matching
306 Barton's joint standard roughness profiles regarded by the International Society for Rock Mechanics
307 (ISRM, 1978). The joint wall compressive strength (*JCS*) was estimated by Schmidt hammer index tests.
308 These tests helped make a quick estimate of the shear strength in situ, which can facilitate the use of
309 Newmark's method in an emergency hazard and risk assessment after an earthquake.

310 It is difficult for a statically stable slope to fail under an earthquake. Earthquakes usually cause slopes to
311 fail in the state of limit equilibrium. For this reason, it is important to characterize the shear strength of
312 the slope accurately. The shear strengths were assigned to the geological units using the results of
313 hundreds of shear tests reported in the references provided in Table 1. We assigned the original shear
314 strengths to the geological units, instead of increasing them to render the cells statically stable, as Jibson
315 et al. (1998, 200) did. This would have changed the statically stable level of the entire study area,
316 especially the slopes in the state of limit equilibrium. In addition, we considered the size effect of the
317 potential slide surface, which could yield a lower F_S and, in turn, a higher displacement. However, the
318 inventory of landslides was used to calibrate the predicted displacements, and the confidence levels
319 indicated by the certainty factors fitted well with the spatial distribution of coseismic landslides, as shown
320 in the hazard map (Fig. 17).

321 We also ran a conventional Newmark analysis using the assigned strengths, such as friction angle (φ) and
322 cohesion (c), as shown in Table 2. The predicted displacements calculated by the conventional Newmark
323 analysis ranged from 0 cm to 121 cm, compared with 0 cm to 122 cm as obtained by the proposed method.
324 Figure 19 shows the hazard map produced using conventional Newmark analysis. The CF s ranged from
325 -1 to 0.94, indicating a very similar result to that of the proposed method above. However, there were
326 large differences along the Shaba River and upstream of the Niulanjiang River between the methods. By
327 comparing Fig. 17 with Fig. 19, we see that the confidence levels of the proposed method fitted the data
328 better than those of the conventional method, especially near upstream of the Niulanjiang River. The area
329 under the curve (AUC) was employed to compare the performance of the methods. To create an AUC
330 plot, the cumulative area of CF s within each interval of the calculated values, from the maximum to the
331 minimum, was determined as a proportion of the total study area (x-axis) and plotted against the
332 proportion of cumulative landslides falling within those CF s (y-axis) (Miles and Keefer, 2009). A value
333 of 0.5 of the AUC indicates that performance is not better than a random guess and that of 1 indicates
334 perfect performance (Miles and Keefer, 2009). Figure 20 shows the results of the AUC analysis of both
335 methods. The calculated value for the proposed method was 0.58 while that for the conventional
336 Newmark's method was 0.53. That is to say, the method introduced here yielded better results, and is an
337 improvement over the conventional Newmark analysis.

338

339 **5 Conclusion**

340 Newmark's method is a useful physical model to estimate the seismic stability of natural slopes. The
341 mapping procedure for data on the 2014 Ludian earthquake shows the feasibility of a Newmark analysis

342 combined with Barton's shear strength criterion. Such a method has practical applications in the
343 assessment of regional seismic hazard. We also considered here the size effect of parameters of shear
344 strength, such as the joint roughness coefficient (*JRC*) and the joint wall compressive strength (*JCS*), in
345 regional analysis. Moreover, linking the Newmark displacements to the certainty factor model improved
346 the utility of Newmark's method to predict the hazard posed by coseismic landslides. Finally, the results
347 of an AUC analysis indicate that the proposed method is more reliable than the conventional Newmark's
348 method.

349

350 Data availability. The digital geological map hosted by the China Geological Survey (CGS) can be made
351 available upon request. The pre-earthquake satellite images are publicly available from Google Earth (last
352 access: 30 January 2014). The 0.2-m high-resolution post-earthquake aerial images from the Digital
353 Mountain and Remote Sensing Applications Center, Institute of Mountain Hazards and Environment,
354 Chinese Academy of Sciences, and Beijing Anxiang Power Technology Co., LTD. are restricted and
355 cannot be accessed publicly but may be requested from the corresponding author. The 30 m × 30 m
356 ASTER Global Digital Elevation Model is distributed by NASA EOSDIS Land Processes DAAC
357 (<https://doi.org/10.5067/ASTER/ASTGTM.002>, last access: 16 July 2018). The dataset of the strong-
358 motion stations is provided by the China Earthquake Data Center (<http://data.earthquake.cn>, last access:
359 16 June 2016).

360

361 Author contributions. SQ initiated and led this research. MZ designed the analytical framework of this
362 study, produced maps and figures, performed the data analysis and interpretation, and wrote the paper.

363 YZ helped interpret landslides and collect the records of the strong-motion stations. SQ, ZS, and BSZ
364 reviewed and edited the paper.

365

366 **Competing interests.** The authors declare that they have no conflict of interest.

367

368 **Acknowledgements.** This **research was** supported by the National Natural Science Foundation of China
369 **(Grant Nos. 41825018, 41672307, and 41807273), the** Science and Technology Service Network
370 **Initiative (Grant No. KFJ-EW-STS-094), and the** China Scholarship Council (No. 201704910537).

371

372 **Review statement.** This paper was edited by Mario Parise and reviewed by two anonymous referees.

373

374 **References**

- 375 Alejano, L. R., González, J. and Muralha, J.: Comparison of different techniques of tilt testing and basic
376 friction angle variability assessment, *Rock Mech. Rock Eng.*, **45**, 1023-1035,
377 <https://xs.scihub.ltd/https://doi.org/10.1007/s00603-012-0265-7>, 2012.
- 378 Alejano, L. R., Perucho, Á., Olalla, C. and Jiménez, R. (Eds.): Rock engineering and rock mechanics:
379 structures in and on rock masses, CRC Press/Balkema, Leiden, the Netherlands, 1536 pp., 2014.
- 380 Ambraseys, N. N. and Menu, J. M.: Earthquake-induced ground displacements, *Earthquake Eng. Struct.*
381 *Dyn.*, **16**, 985-1006, <https://doi.org/10.1002/eqe.4290160704>, 1988.
- 382 Bandis, S., Lumsden, A. C. and Barton, N. R.: Experimental studies of scale effects on the shear behaviour
383 of rock joints, *Int. J. Rock Mech. Min. Sci. & Geomech. Abstr.*, **18**, 1-21,
384 [https://doi.org/10.1016/0148-9062\(81\)90262-X](https://doi.org/10.1016/0148-9062(81)90262-X), 1981.
- 385 Bandis, S. C., Lumsden, A. C. and Barton, N. R.: Fundamentals of rock joint deformation, *Int. J. Rock*
386 *Mech. Min. Sci. & Geomech. Abstr.*, **20**, 249-268, [https://doi.org/10.1016/0148-9062\(83\)90595-8](https://doi.org/10.1016/0148-9062(83)90595-8),
387 1983.
- 388 Barton, N.: Review of a new shear-strength criterion for rock joints, *Eng. Geol.*, **7**, 287-332,
389 [https://doi.org/10.1016/0013-7952\(73\)90013-6](https://doi.org/10.1016/0013-7952(73)90013-6), 1973.
- 390 Barton, N. and Bandis, S.: Effects of block size on the shear behavior of jointed rock, in: *Proceedings of*
391 *the 23rd US Symposium on Rock Mechanics (USRMS), Berkeley, California, USA, 25-27 August*
392 *1982*, 739-760, 1982.
- 393 Barton, N. and Choubey, V.: The shear strength of rock joints in theory and practice, *Rock Mech.*, **10**, 1-
394 54, <https://xs.scihub.ltd/https://doi.org/10.1007/BF01261801>, 1977.

- 395 Bilgin, H. A. and Pasamehmetoglu, A. G.: Shear behaviour of shale joints under heat in direct shear, in:
396 [Proceedings of the International symposium on rock joints, Leon, Norway, 4-6 June 1990](#), 179-183,
397 1990.
- 398 Bray, J. D. and Travasarou, T.: Simplified procedure for estimating earthquake-induced deviatoric slope
399 displacements, [J. Geotech. Geoenviron., 133](#), 381-392, [https://doi.org/10.1061/\(ASCE\)1090-](https://doi.org/10.1061/(ASCE)1090-0241(2007)133:4(381))
400 [0241\(2007\)133:4\(381\)](https://doi.org/10.1061/(ASCE)1090-0241(2007)133:4(381)), 2007.
- 401 Burrough, P. A. and McDonnell, R. A. (Eds.): Principles of geographical information systems (2nd
402 Edition), Oxford University Press, [Oxford, UK](#), 1998.
- 403 Chang, Z. F., Chang, H., Yang, S. Y., Chen, G. and Li, J. L.: Characteristics and formation mechanism
404 of large rock avalanches triggered by the Ludian Ms6.5 earthquake at Hongshiyuan and Ganjiazhai,
405 [Seismology and Geology, 39](#), 1030-1047, 2017 (in Chinese with English abstract).
- 406 Chen, X. L., Ran, H. L. and Yang, W. T.: Evaluation of factors controlling large earthquake-induced
407 landslides by the Wenchuan earthquake, [Nat. Hazards Earth Syst. Sci., 12](#), 3645-3657,
408 <https://doi.org/10.5194/nhess-12-3645-2012>, 2012.
- 409 Chen, X. L., Zhou, Q. and Liu, C. G.: Distribution pattern of coseismic landslides triggered by the 2014
410 Ludian, Yunnan, China Mw6.1 earthquake: special controlling conditions of local topography,
411 [Landslides, 12](#), 1159-1168, <https://xs.scihub.ltd/https://doi.org/10.1007/s10346-015-0641-y>, 2015.
- 412 Chen, X. L., Liu, C. G., Wang, M. M. and Zhou, Q.: Causes of unusual distribution of coseismic landslides
413 triggered by the Mw 6.1 2014 Ludian, Yunnan, China earthquake, [J. Asian Earth Sci., 159](#), 17-23,
414 <https://doi.org/10.1016/j.jseaes.2018.03.010>, 2018.

415 Chen, X. L., Liu, C. G. and Wang, M. M.: A method for quick assessment of earthquake-triggered
416 landslide hazards: a case study of the Mw6. 1 2014 Ludian, China earthquake, *Bull. Eng. Geol.*
417 *Environ.*, 78, 2449-2458, <https://xs.scihub.ltd/https://doi.org/10.1007/s10064-018-1313-7>, 2019.
418 *China Earthquake Data Center: <http://data.earthquake.cn>*, last access: 16 June 2016.

419 Clough, R. W. and Chopra, A. K.: Earthquake stress analysis in earth dams, *ASCE J. Eng. Mech. Div.*,
420 92, 197-211, 1966.

421 Coulson, J. H.: Shear strength of flat surfaces in rock, in: *Proceedings of the 13th Symposium on Rock*
422 *Mechanics, Urbana, Illinois, USA, August 30-September 1, 1971*, 77-105, 1972.

423 Dai, F. C., Xu, C., Yao, X., Xu, L., Tu, X. B. and Gong, Q. M.: Spatial distribution of landslides triggered
424 by the 2008 Ms 8.0 Wenchuan earthquake, China, *J. Asian Earth Sci.*, 40, 883-895,
425 <https://doi.org/10.1016/j.jseaes.2010.04.010>, 2011.

426 Geological Engineering Handbook Editorial Committee (Ed.): *Geological Engineering Handbook*, China
427 *Architecture & Building Press, Beijing, China, 2018 (in Chinese)*.

428 Giusepone, F. and da Silva, L. A. A.: Hoek & Brown and Barton & Bandis Criteria Applied to a Planar
429 Sliding at a Dolomite Mine in Gandarela Synclinal, in: *Proceedings of the ISRM Conference on*
430 *Rock Mechanics for Natural Resources and Infrastructure-SBMR 2014, Goiania, Brazil, 9-13*
431 *September 2014, ISRM-SBMR-2014-009*, 2014.

432 Gu, D. Z. (Ed.): *Engineering geomechanics of rock mass*, Science Press, Beijing, China, 1979 (in Chinese).

433 Harp, E. L. and Jibson, R. W.: Landslides triggered by the 1994 Northridge, California, earthquake, *Bull.*
434 *Seismol. Soc. Am.*, 86, S319-S332, 1996.

435 Heckerman, D.: Probabilistic interpretations for MYCIN's certainty factors, *Mach. Intell. Patt. Rec.*, 4,
436 167-196, <https://doi.org/10.1016/B978-0-444-70058-2.50017-6>, 1986.

437 Hsieh, S. Y. and Lee, C. T.: Empirical estimation of the Newmark displacement from the Arias intensity
438 and critical acceleration, *Eng. Geol.*, 122, 34-42, <https://doi.org/10.1016/j.enggeo.2010.12.006>, 2011.

439 Hoek, E. and Bray, J. D. (Eds.): Rock slope engineering (3rd editon), Taylor & Francis, Abingdon, UK,
440 1981.

441 **International Society for Rock Mechanics (ISRM): International society for rock mechanics commission**
442 **on standardization of laboratory and field tests:** Suggested methods for the quantitative description
443 of discontinuities in rock masses, *Int. J. Rock Mech. Min. Sci. & Geomech. Abstr.*, 15, 319-368,
444 [https://doi.org/10.1016/0148-9062\(78\)91472-9](https://doi.org/10.1016/0148-9062(78)91472-9), 1978.

445 Jaeger, J. C. and Cook, N. G. W. (Eds.): Fundamentals of Rock Mechanics, Methuen, London, UK, 513
446 pp., 1969.

447 Jibson, R. W.: Predicting earthquake-induced landslide displacements using Newmark's sliding block
448 analysis, *Transp. Res. Rec.*, 1411, 9-17, 1993.

449 Jibson, R. W.: Regression models for estimating coseismic landslide displacement, *Eng. Geol.*, 91, 209-
450 218, <https://doi.org/10.1016/j.enggeo.2007.01.013>, 2007.

451 Jibson, R. W.: Methods for assessing the stability of slopes during earthquakes-A retrospective, *Eng.*
452 *Geol.*, 122, 43-50, <https://doi.org/10.1016/j.enggeo.2010.09.017>, 2011.

453 Jibson, R. W., Harp, E. L. and Michael, J. A.: A method for producing digital probabilistic seismic
454 landslide hazard maps: an example from the Los Angeles, California, area, U.S. Geological Survey,
455 **Denver, USA, Open File Rep. 98-113, 17 pp., 1998.**

456 Jibson, R. W., Harp, E. L. and Michael, J. A.: A method for producing digital probabilistic seismic
457 landslide hazard maps, *Eng. Geol.*, **58**, 271-289, [https://doi.org/10.1016/S0013-7952\(00\)00039-9](https://doi.org/10.1016/S0013-7952(00)00039-9),
458 2000.

459 Keefer, D. K.: Landslides caused by earthquakes, *Geol. Soc. Am. Bull.*, **95**, 406-421,
460 [https://doi.org/10.1130/0016-7606\(1984\)95<406:LCBE>2.0.CO;2](https://doi.org/10.1130/0016-7606(1984)95<406:LCBE>2.0.CO;2), 1984.

461 Khazai, B. and Sitar, N.: Evaluation of factors controlling earthquake-induced landslides caused by Chi-
462 Chi earthquake and comparison with the Northridge and Loma Prieta events, *Eng. Geol.*, **71**, 79-95,
463 [https://doi.org/10.1016/S0013-7952\(03\)00127-3](https://doi.org/10.1016/S0013-7952(03)00127-3), 2004.

464 Miles, S. B. and Keefer, D. K.: Evaluation of CAMEL-comprehensive areal model of earthquake-induced
465 landslides, *Eng. Geol.*, **104**, 1-15, <https://doi.org/10.1016/j.enggeo.2008.08.004>, 2009.

466 NASA/METI/AIST/Japan Spacesystems, and U.S./Japan ASTER Science Team: ASTER Global Digital
467 Elevation Model version **002**, NASA EOSDIS Land Processes DAAC,
468 <https://doi.org/10.5067/ASTER/ASTGTM.002>, 2009.

469 Newmark, N. M.: Effects of earthquakes on dams and embankments, *Geotechnique*, **15**, 139-160, 1965.

470 Pradel, D., Smith, P. M., Stewart, J. P. and Raad, G.: Case history of landslide movement during the
471 Northridge earthquake, *J. Geotech. Geoenviron. Eng.*, **131**, 1360-1369,
472 [https://doi.org/10.1061/\(ASCE\)1090-0241\(2005\)131:11\(1360\)](https://doi.org/10.1061/(ASCE)1090-0241(2005)131:11(1360)), 2005.

473 Priest, S. D. (Ed.): *Discontinuity analysis for rock engineering*, Chapman & Hall, London, UK, 1993.

474 Qi, S. W., Xu, Q., Lan, H. X., Zhang, B. and Liu, J. Y.: Spatial distribution analysis of landslides triggered
475 by 2008.5.12 Wenchuan Earthquake, China, *Eng. Geol.*, **116**, 95-108,
476 <https://doi.org/10.1016/j.enggeo.2010.07.011>, 2010.

477 Qi, S. W., Xu, Q., Zhang, B., Zhou, Y. D., Lan, H. X. and Li, L. H.: Source characteristics of long runout
478 rock avalanches triggered by the 2008 Wenchuan earthquake, China, *J. Asian Earth Sci.*, **40**, 896-
479 906, <https://doi.org/10.1016/j.jseaes.2010.05.010>, 2011.

480 Qi, S. W., Yan, C. G. and Liu, C. L.: Two typical types of earthquake triggered landslides and their
481 mechanisms, in: *Proceedings of the 11th International and 2nd North American Symposium on*
482 *Landslides and Engineered Slopes, Banff, Canada, 3-8 June 2012*, 1819-1823, 2012.

483 Rathje, E. M. and Antonakos, G.: A unified model for predicting earthquake-induced sliding
484 displacements of rigid and flexible slopes, *Eng. Geol.*, **122**, 51-60,
485 <https://doi.org/10.1016/j.enggeo.2010.12.004>, 2011.

486 Rathje, E. M. and Saygili, G.: Probabilistic assessment of earthquake-induced sliding displacements of
487 natural slopes, *Bulletin of the New Zealand Society for Earthquake Engineering*, **42**, 18-27,
488 <https://doi.org/10.5459/bnzsee.42.1.18-27>, 2009.

489 Saygili, G. and Rathje, E. M.: Empirical predictive models for earthquake-induced sliding displacements
490 of slopes, *J. Geotech. Geoenviron. Eng.*, **134**, 790-803, [https://doi.org/10.1061/\(ASCE\)1090-
491 0241\(2008\)134:6\(790\)](https://doi.org/10.1061/(ASCE)1090-0241(2008)134:6(790)), 2008.

492 Shortliffe, E. H. and Buchanan, B. G.: A model of inexact reasoning in medicine, *Math. Biosci.*, **23**, 351-
493 379, [https://doi.org/10.1016/0025-5564\(75\)90047-4](https://doi.org/10.1016/0025-5564(75)90047-4), 1975.

494 Singh, T. N., Kainthola, A. and Venkatesh, A.: Correlation between point load index and uniaxial
495 compressive strength for different rock types, *Rock Mech. Rock Eng.*, **45**, 259-264,
496 <https://xs.scihub.ltd/https://doi.org/10.1007/s00603-011-0192-z>, 2012.

497 Tang, C., Ma, G., Chang, M., Li, W., Zhang, D., Jia, T. and Zhou, Z.: Landslides triggered by the 20 April
498 2013 Lushan earthquake, Sichuan Province, China, *Eng. Geol.*, 187, 45-55,
499 <https://doi.org/10.1016/j.enggeo.2014.12.004>, 2015.

500 Terzaghi, K.: Mechanism of landslides, in: Application of Geology to Engineering Practice, edited by:
501 Paige, S., Geological Society of America, New York, NY, USA, 83-123,
502 <https://doi.org/10.1130/Berkey.1950.83>, 1950.

503 Watson, D. F. and Philip, G. M.: A Refinement of Inverse Distance Weighted Interpolation,
504 *Geoprocessing*, 2, 315-327, 1985.

505 Weibull, W. (Ed.): A Statistical Theory of the Strength of Materials, *Generalstabens Litografiska Anstalts*
506 *Förlag*, Stockholm, Sweden, 1939.

507 Wieczorek, G. F., Wilson, R. C. and Harp, E. L.: Map showing slope stability during earthquakes in San
508 Mateo County, California, U.S. Geological Survey, Denver, USA, Map I-1257-E,
509 <https://doi.org/10.3133/i1257E>, 1985.

510 Wilson, R. C. and Keefer, D. K.: Dynamic analysis of a slope failure from the 6 August 1979 Coyote
511 Lake, California, earthquake, *Bull. Seismol. Soc. Am.*, 73, 863-877, 1983.

512 Xu, C., Xu, X., Zhou, B., and Yu, G.: Revisions of the M 8.0 Wenchuan earthquake seismic intensity
513 map based on co-seismic landslide abundance, *Nat. Hazards*, 69, 1459-1476,
514 <https://xs.scihub.ltd/https://doi.org/10.1007/s11069-013-0757-0>, 2013.

515 Yong, R., Ye, J., Liang, Q. F., Huang, M. and Du, S. G.: Estimation of the joint roughness coefficient
516 (JRC) of rock joints by vector similarity measures, *Bull. Eng. Geol. Environ.*, 77, 735-749,
517 <https://xs.scihub.ltd/https://doi.org/10.1007/s10064-016-0947-6>, 2018.

518 Yuan, R. M., Tang, C. L., Hu, J. C., and Xu, X. W.: Mechanism of the Donghekou landslide triggered by
519 the 2008 Wenchuan earthquake revealed by discrete element modeling, *Nat. Hazards Earth Syst.*
520 *Sci.*, 14, 1195-1205, <https://doi.org/10.5194/nhess-14-1195-2014>, 2014.

521 Zhou, S. H., Chen, G. Q. and Fang, L. G.: Distribution pattern of landslides triggered by the 2014 Ludian
522 earthquake of China: Implications for regional threshold topography and the seismogenic fault
523 identification, *ISPRS Int. J. Geo-Inf.*, 5, 46, <https://doi.org/10.3390/ijgi5040046>, 2016.

524

525 **Figure Captions**

526 **Fig. 1.** Map of the study area showing the inventoried landslides.

527 **Fig. 2.** Geological map of the study area showing lithology and faults.

528 **Fig. 3.** Conceptual sliding-block model of Newmark analysis.

529 **Fig. 4.** A schematic diagram showing shadow unloading joints in the slope.

530 **Fig. 5.** Demonstration of the Newmark analysis algorithm (adapted from Wilson and Keefer, 1983; Jibson
531 et al., 1998, 2000)

532 **Fig. 6.** Slope map derived from the DEM of the study area.

533 **Fig. 7.** Schematic map showing the angle (α) for slopes steeper than 60° . σ_{1f} and σ_3 are the major
534 and minor principal stress in the state of limit equilibrium, respectively. ϕ_b is the basic friction angle.

535 **Fig. 8.** JRC_n component of shear strength assigned to rock types in the study area.

536 **Fig. 9.** JCS_n component of shear strength assigned to rock types in the study area.

537 **Fig. 10.** Basic-friction-angle (ϕ_b) component of shear strength assigned to rock types in the study area.

538 **Fig. 11.** Unit weight (γ) assigned to rock types in the study area.

539 **Fig. 12.** Static factor-of-safety map of the study area.

540 **Fig. 13.** Map showing critical accelerations in the study area.

541 **Fig. 14.** Locations of strong-motion stations.

542 **Fig. 15.** Contour map of peak ground acceleration (PGA) produced by the Ludian earthquake in the
543 study area. PGA values shown are in g .

544 **Fig. 16.** Map showing predicted displacements in the study area.

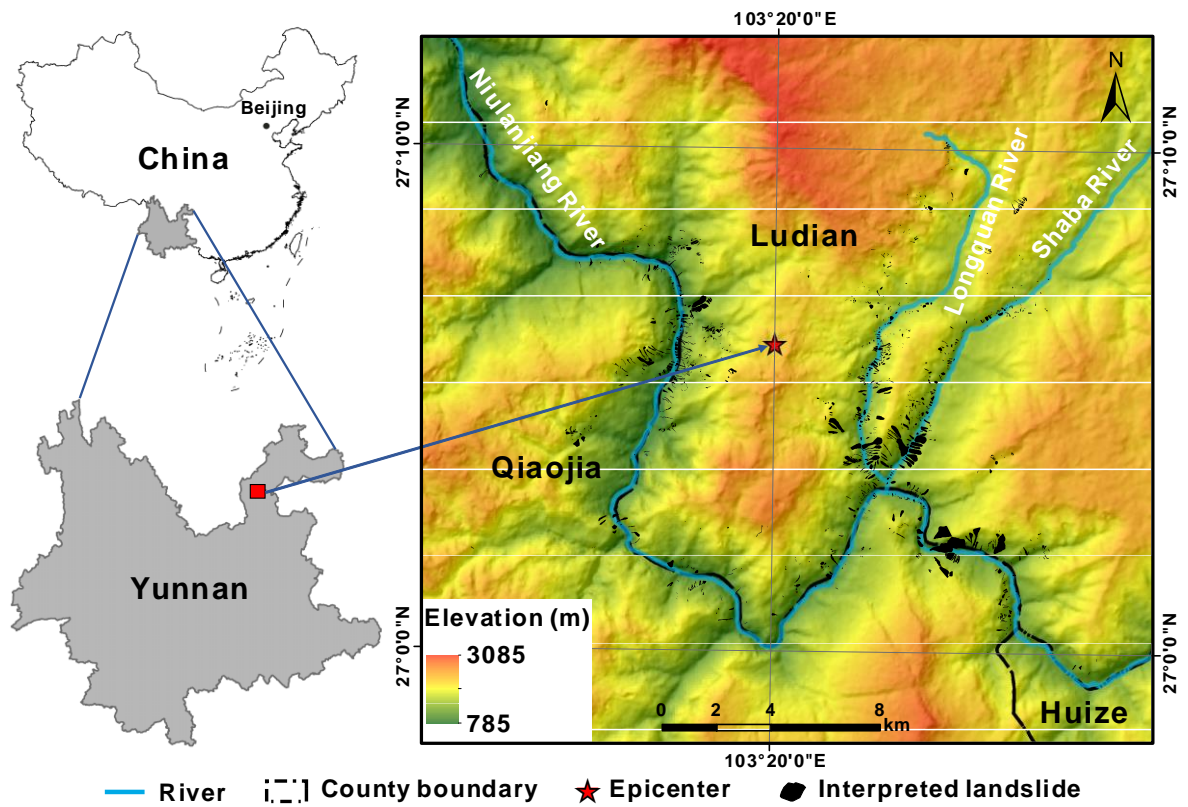
545 **Fig. 17.** Map showing confidence levels of coseismic landslides in the Ludian earthquake using the
546 proposed method. Confidence levels are portrayed in terms of values of CF .

547 **Fig. 18.** Proportion of the area of landslides in each CF value area. A dot shows the CF value of
548 Newmark displacement bin; the red line is the fitting curve of the data using a modified Weibull function.

549 **Fig. 19.** Map showing confidence levels of coseismic landslides in the Ludian earthquake using a
550 conventional Newmark analysis. Confidence levels are portrayed in terms of values of CF .

551 **Fig. 20.** Plots of area under the curve comparing the proposed method with the conventional Newmark's
552 method.

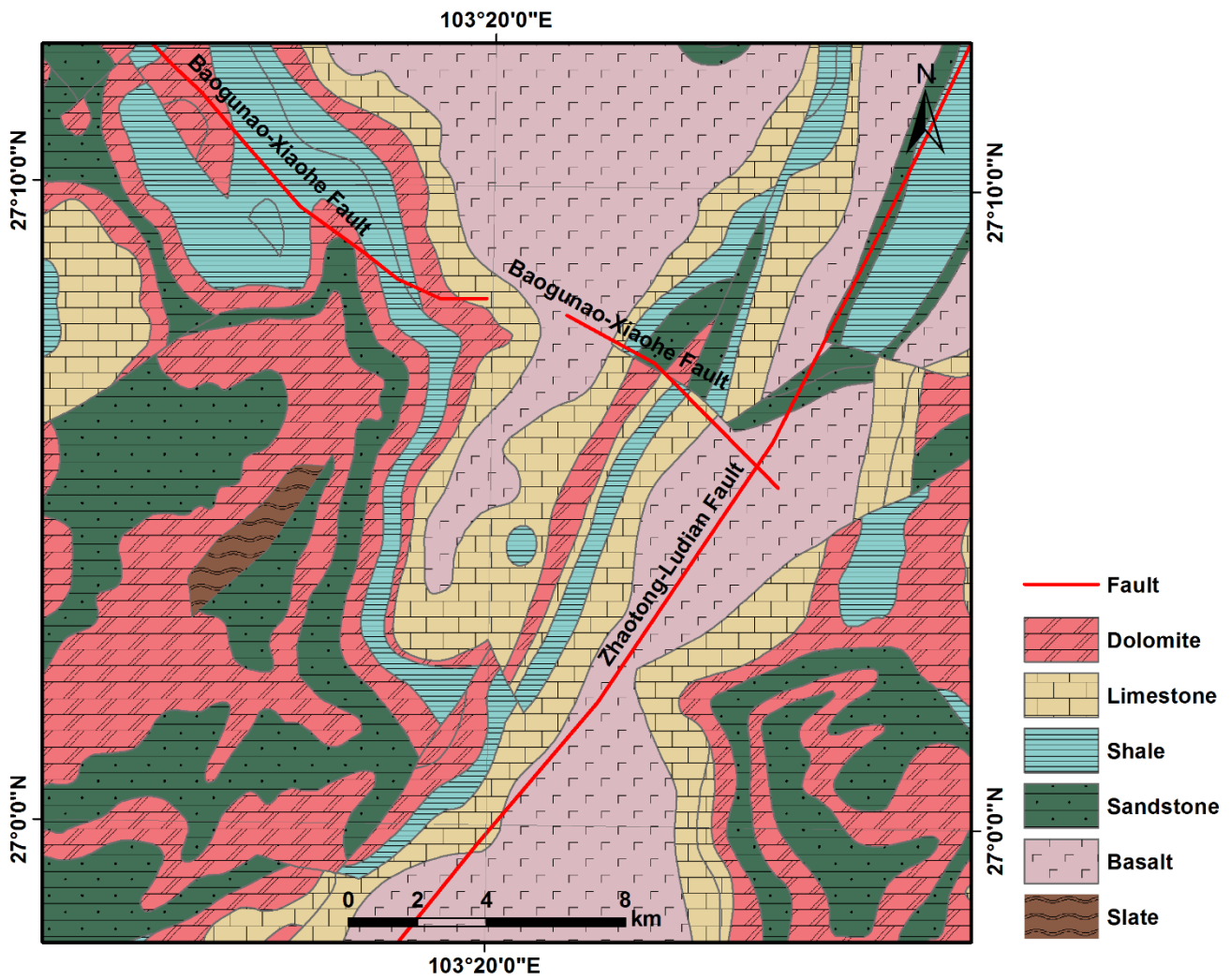
553



554

555 **Fig. 1.** Map of the study area showing the inventoried landslides.

556

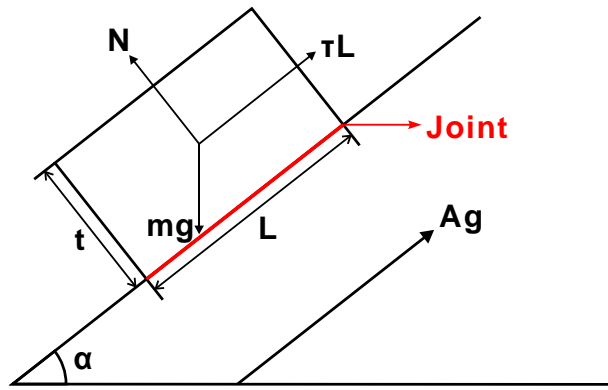


557

558 **Fig. 2.** Geological map of the study area showing lithology and faults.

559

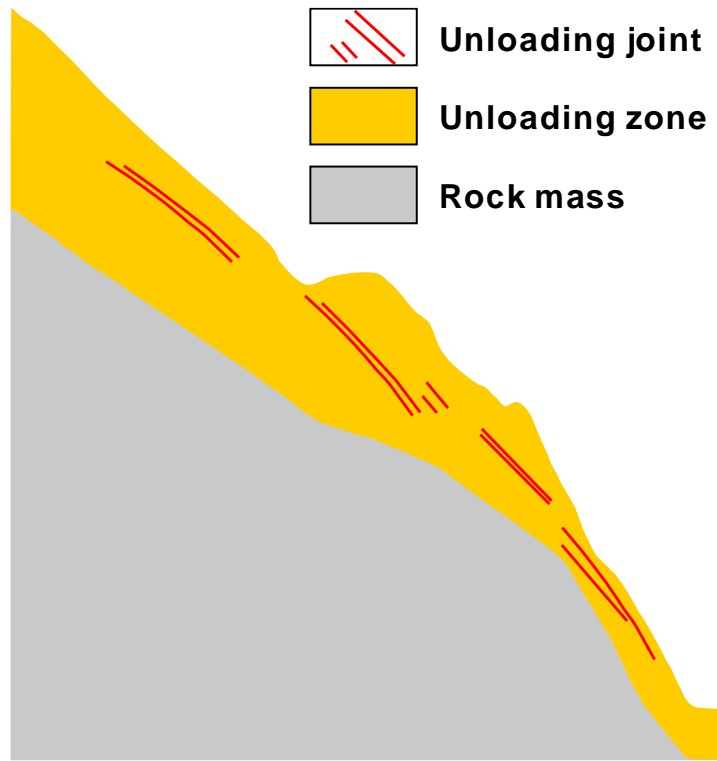
560



561

562 **Fig. 3.** Conceptual sliding-block model of **Newmark** analysis. The potential landslide is modeled as a
 563 **rigid plastic** block resting on an inclined plane at an angle (α) from the horizontal (Jibson et al., 1998,
 564 2000). The base of the block is subjected to an earthquake ground acceleration that is denoted by Ag .

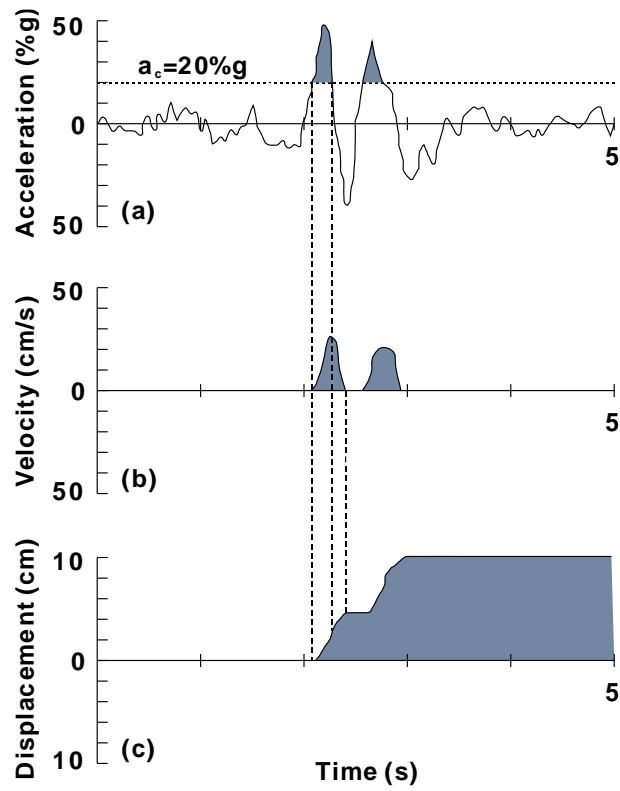
565



566

567 **Fig. 4.** A schematic diagram showing shallow unloading joints in the slope.

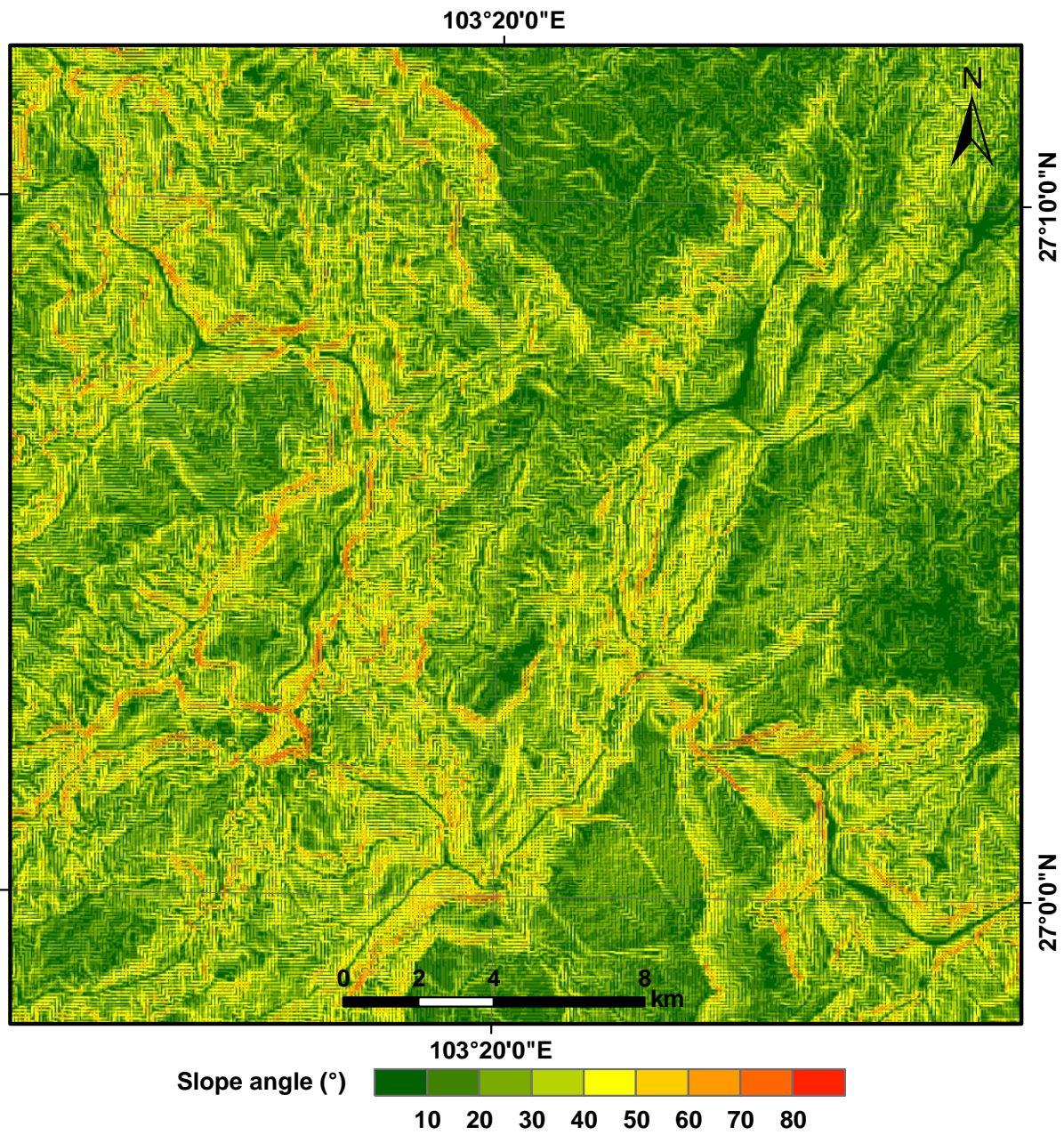
568



569

570 **Fig. 5.** Demonstration of the Newmark analysis algorithm (adapted from Wilson and Keefer, 1983; Jibson
 571 et al., 1998, 2000): (a) Acceleration-time history with critical acceleration (horizontal dotted line) of 20%g
 572 superimposed. (b) Velocity of block versus time. (c) Displacement of block versus time.

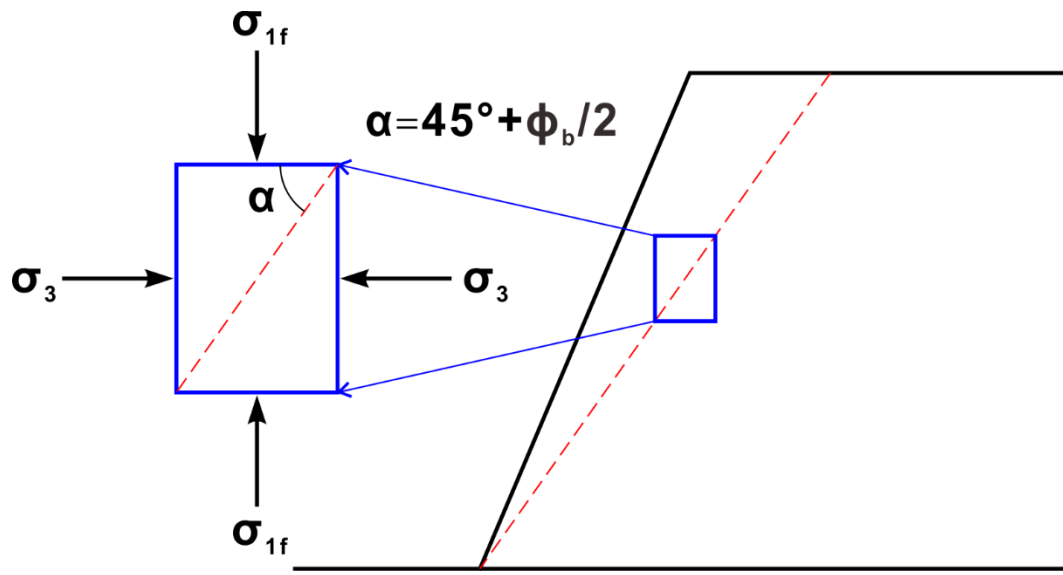
573



574

575 **Fig. 6.** Slope map derived from the DEM of the study area.

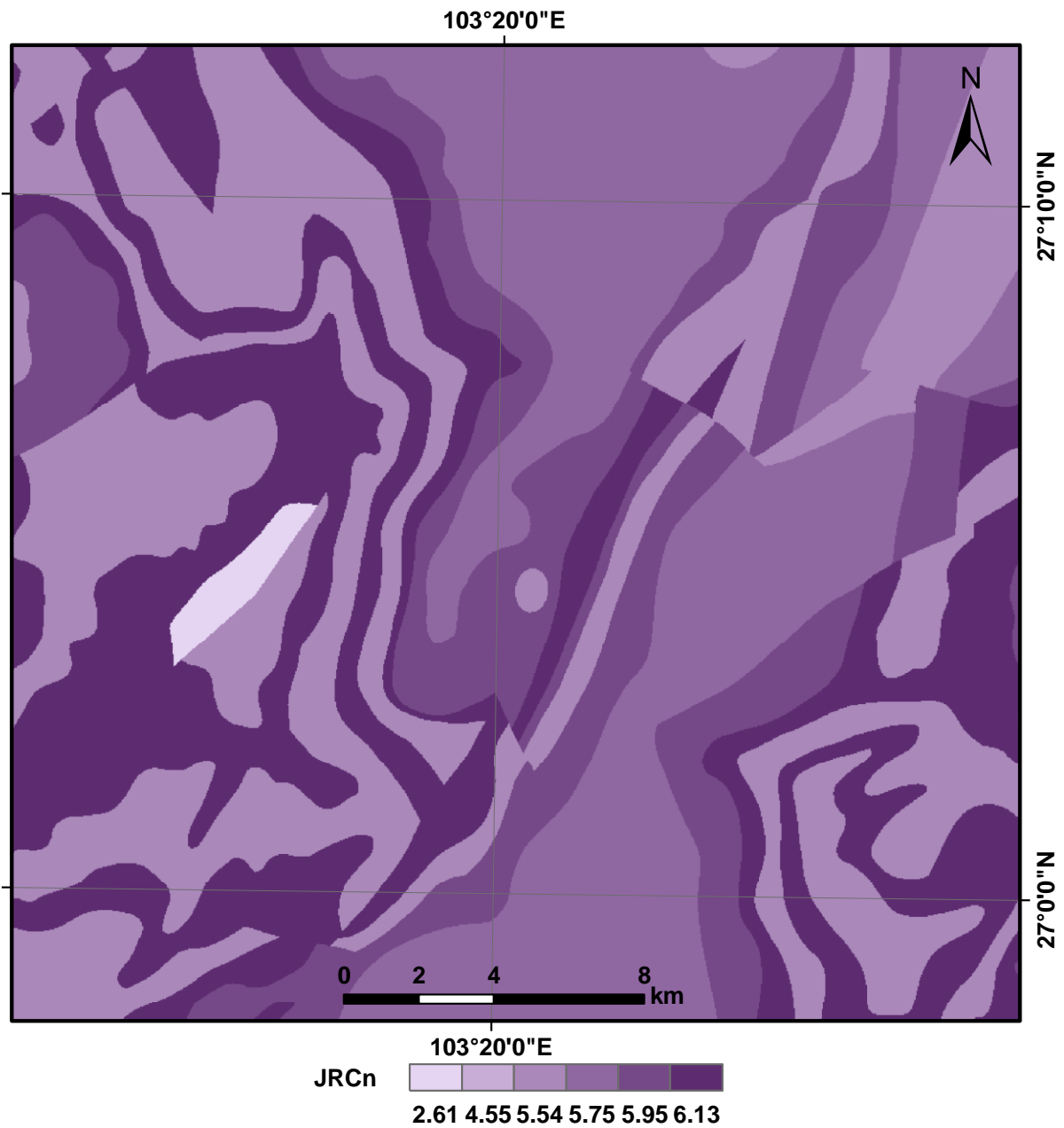
576



577

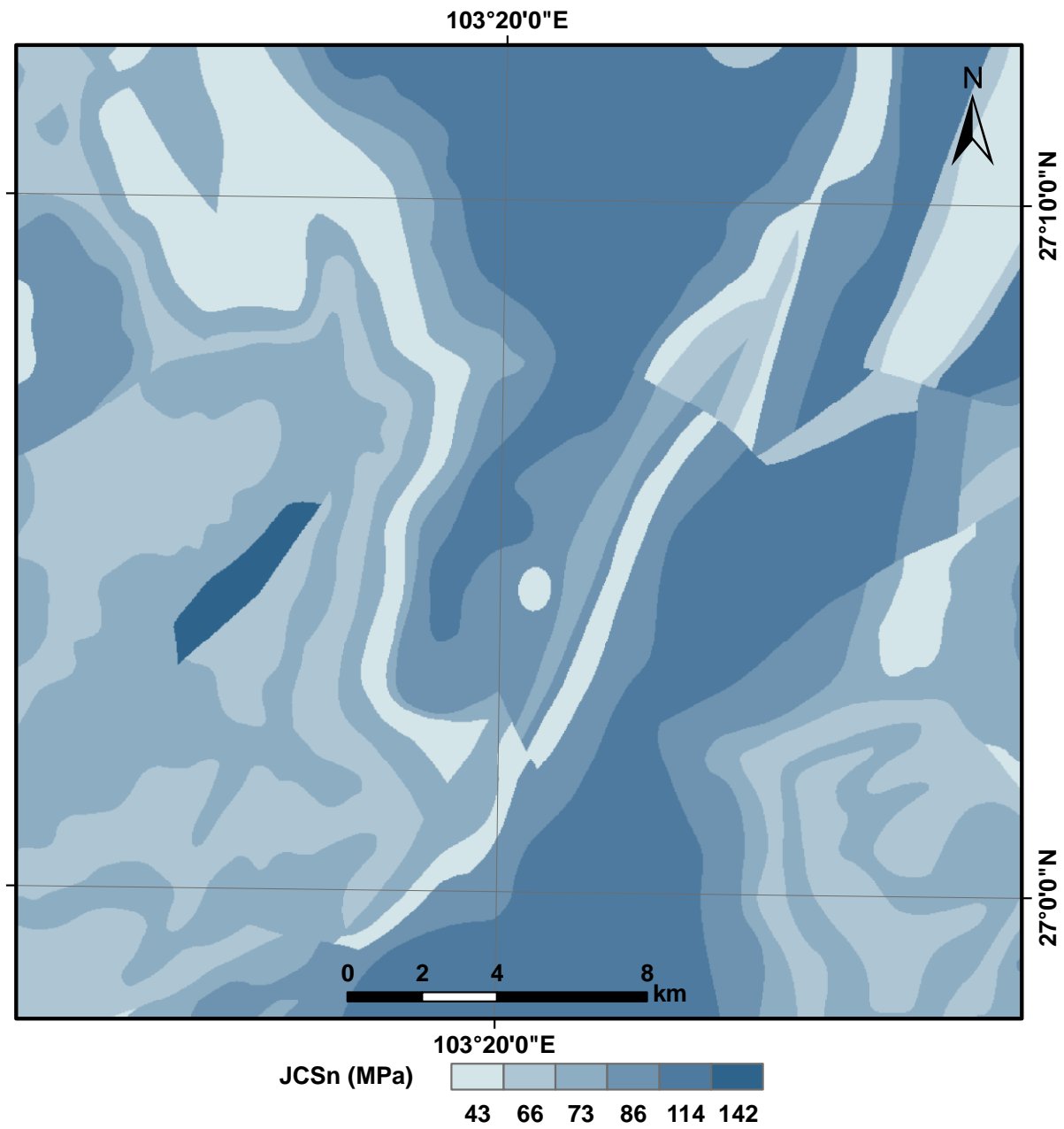
578 **Fig. 7.** Schematic map showing the angle (α) for slopes steeper than 60° . σ_{1f} and σ_3 are the major
 579 and minor principal stress in the state of limit equilibrium, respectively. ϕ_b is the basic friction angle.

580



581

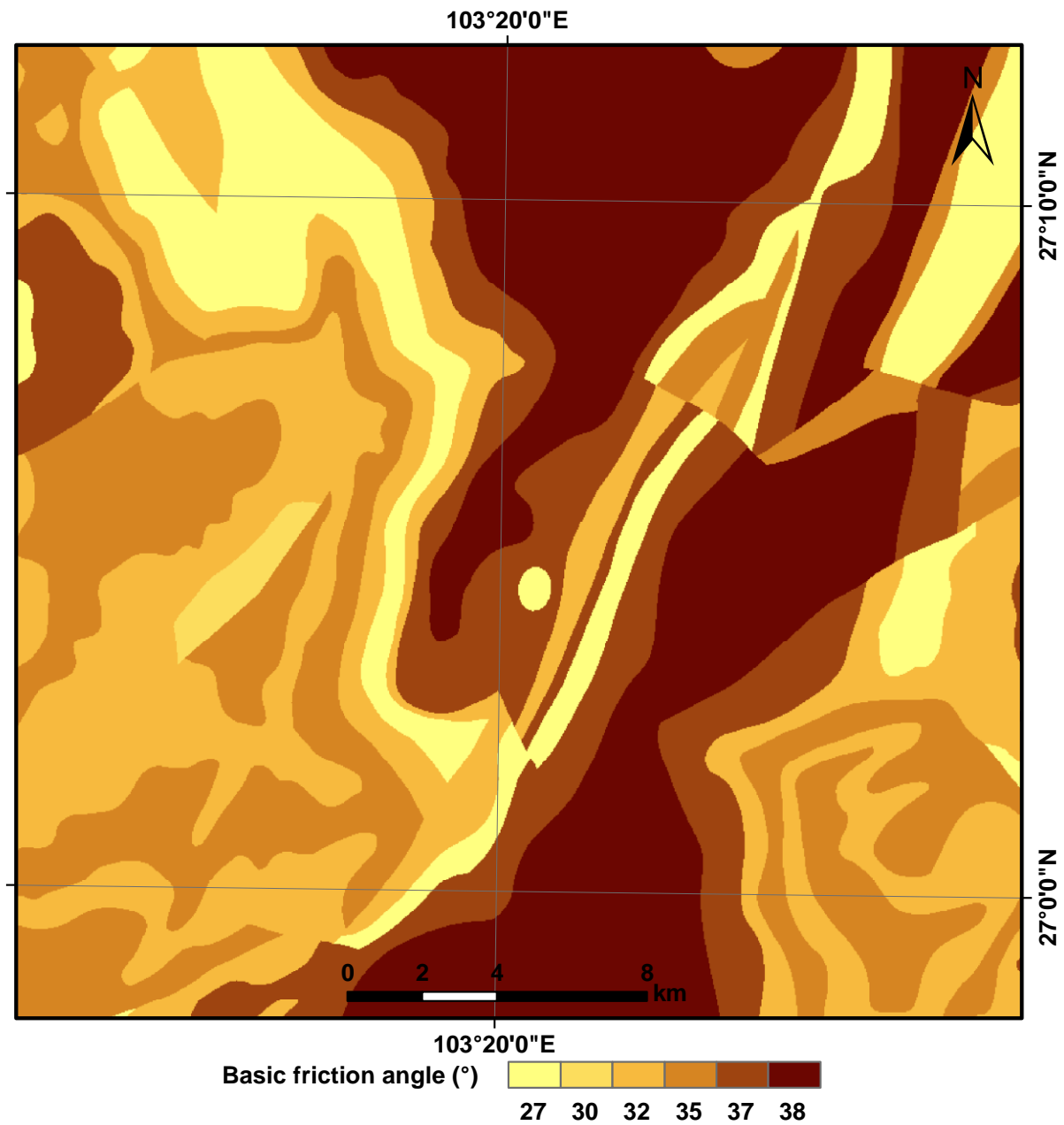
582 **Fig. 8.** JRC_n component of shear strength assigned to rock types in the study area.



583

584 **Fig. 9.** JCS_n component of shear strength assigned to rock types in the study area.

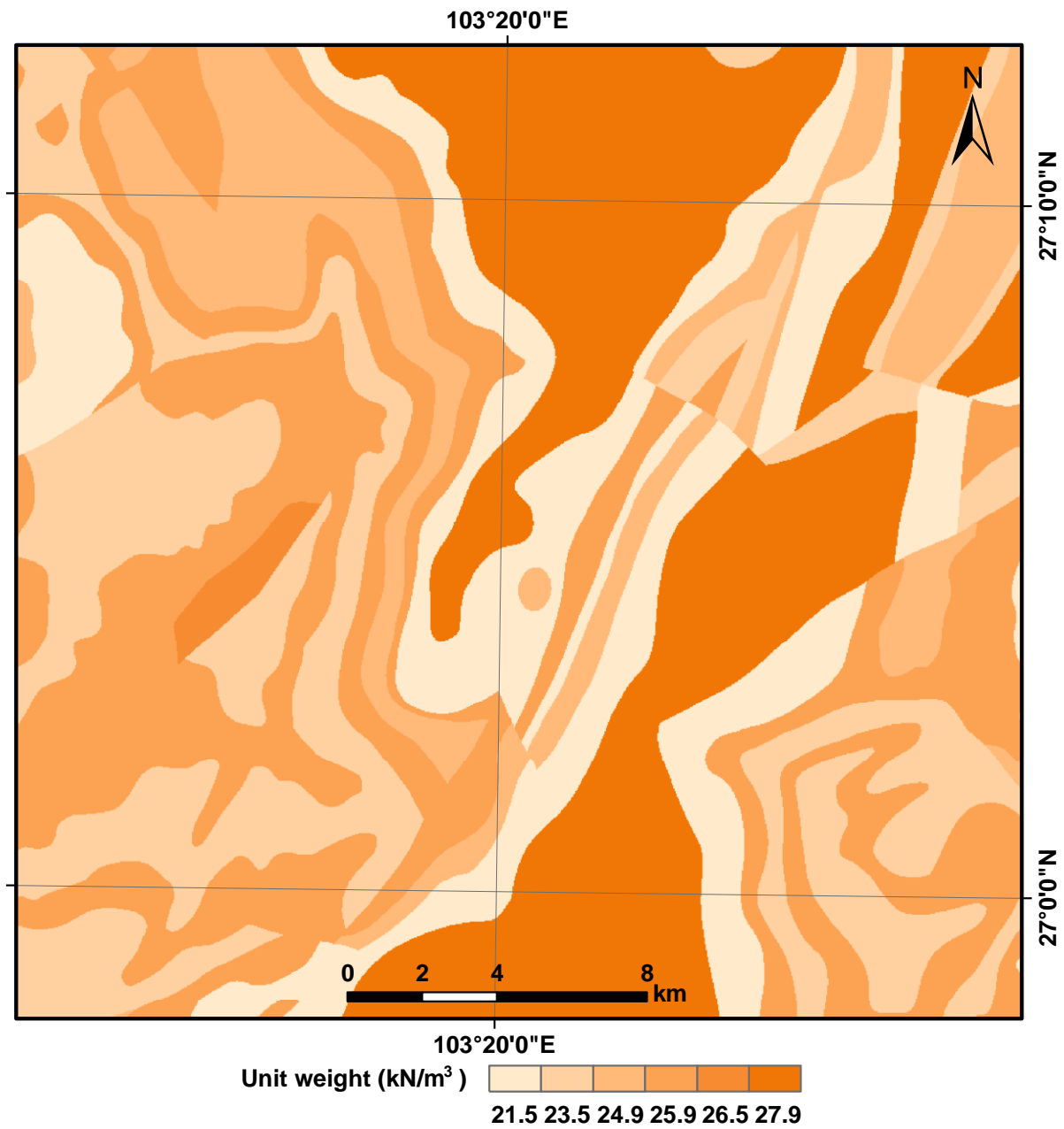
585



586

587 **Fig. 10.** Basic-friction-angle (ϕ_b) component of shear strength assigned to rock types in the study area.

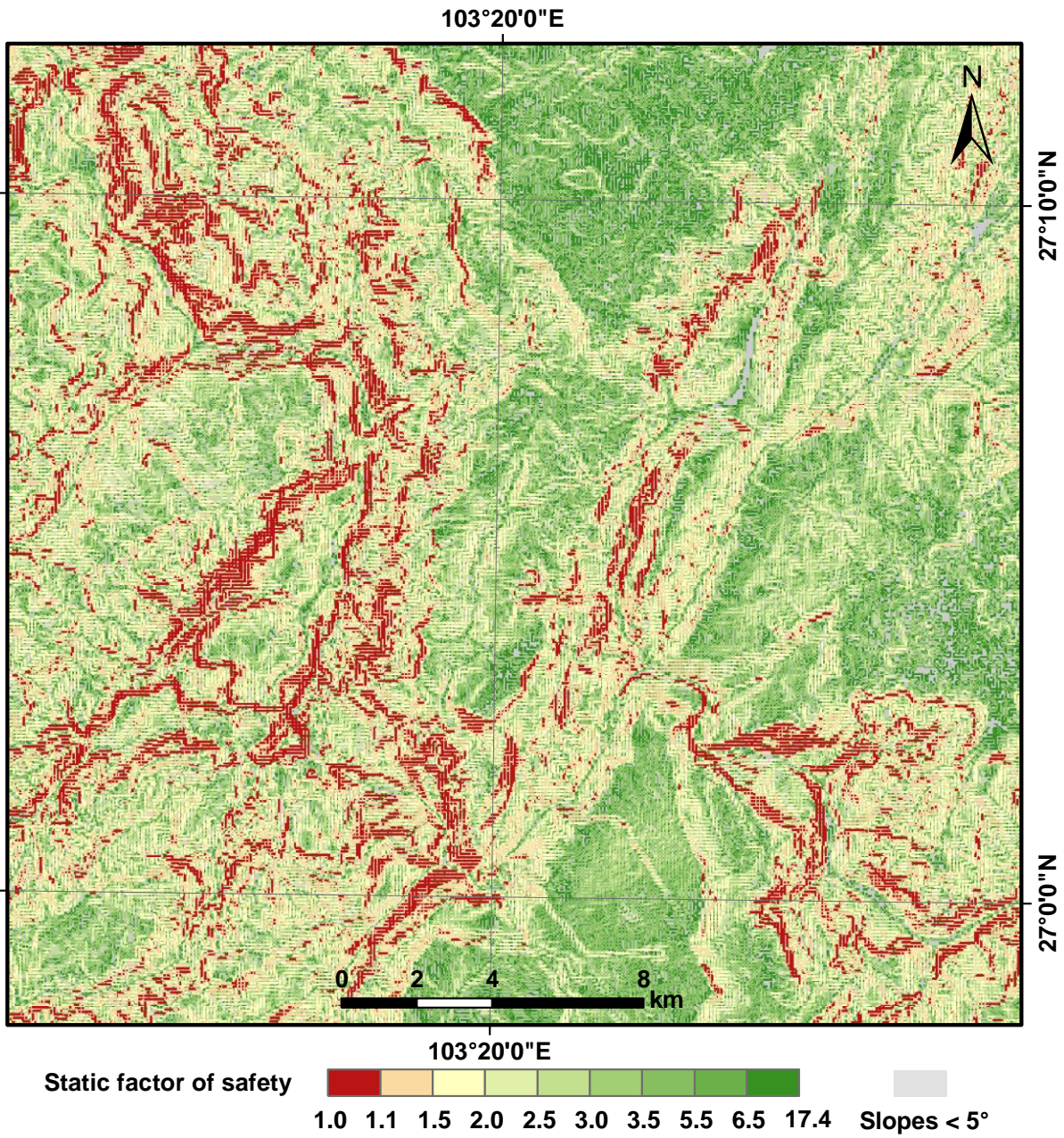
588



589

590 **Fig. 11.** Unit weight (γ) assigned to rock types in the study area.

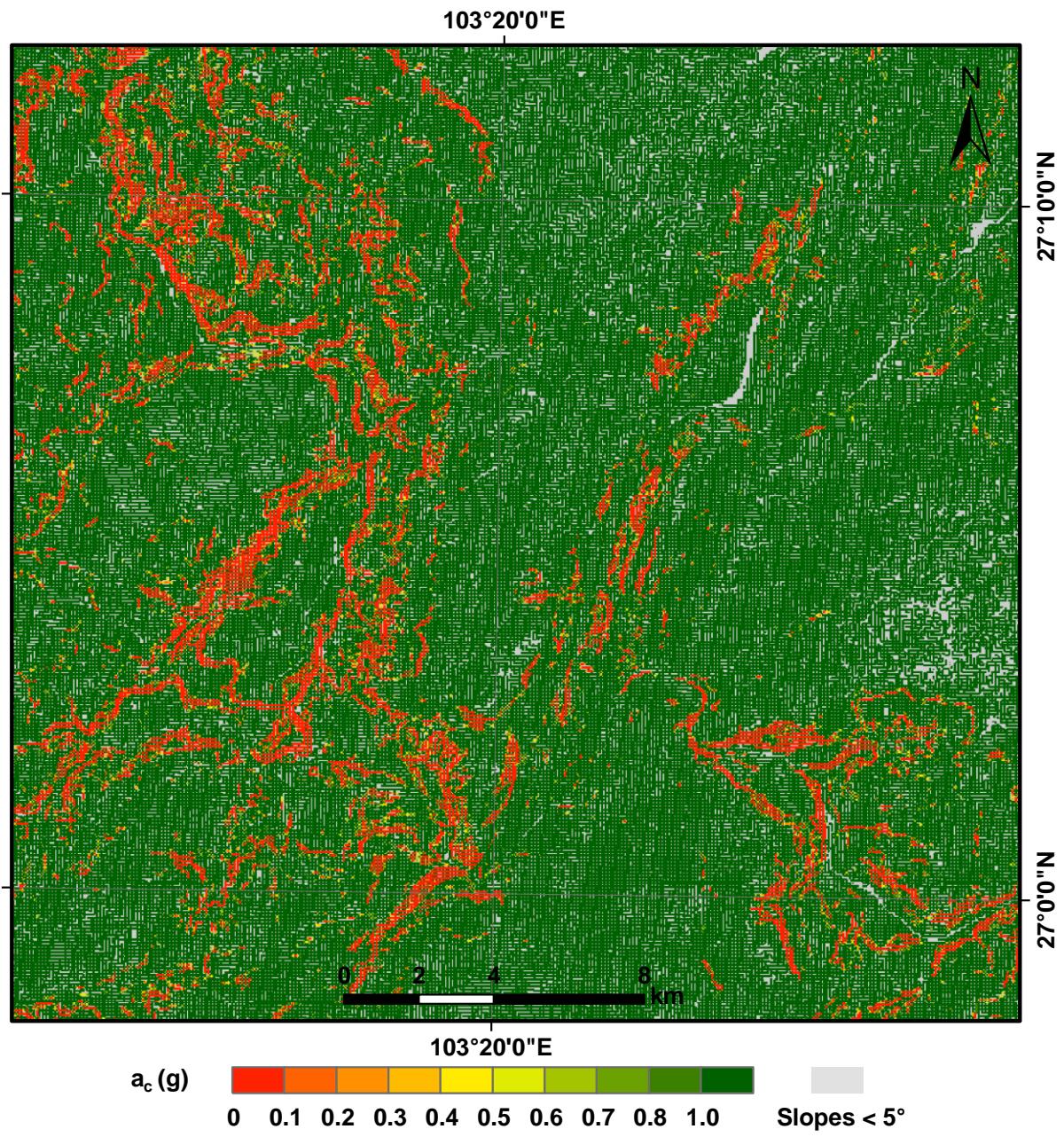
591



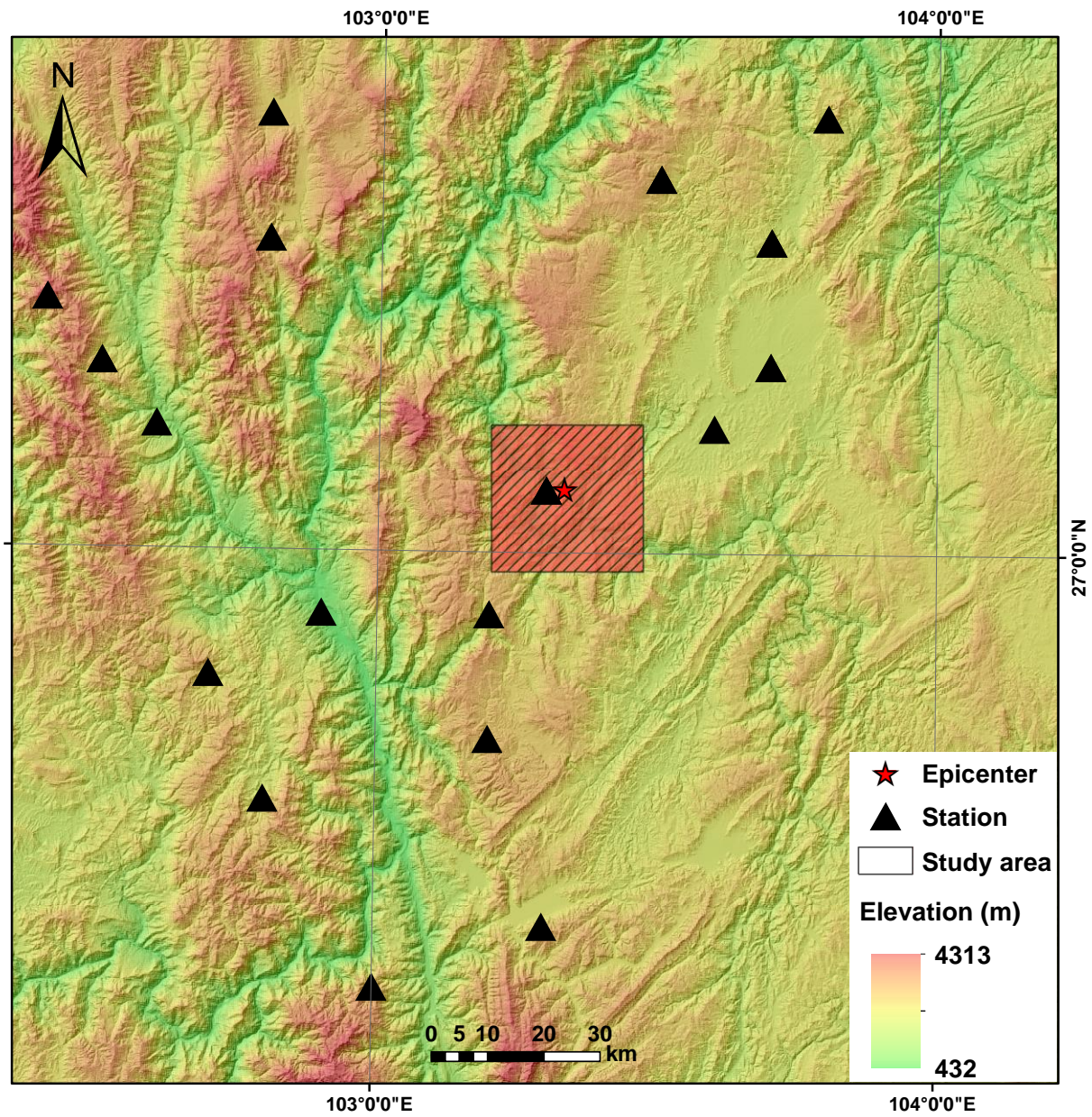
592

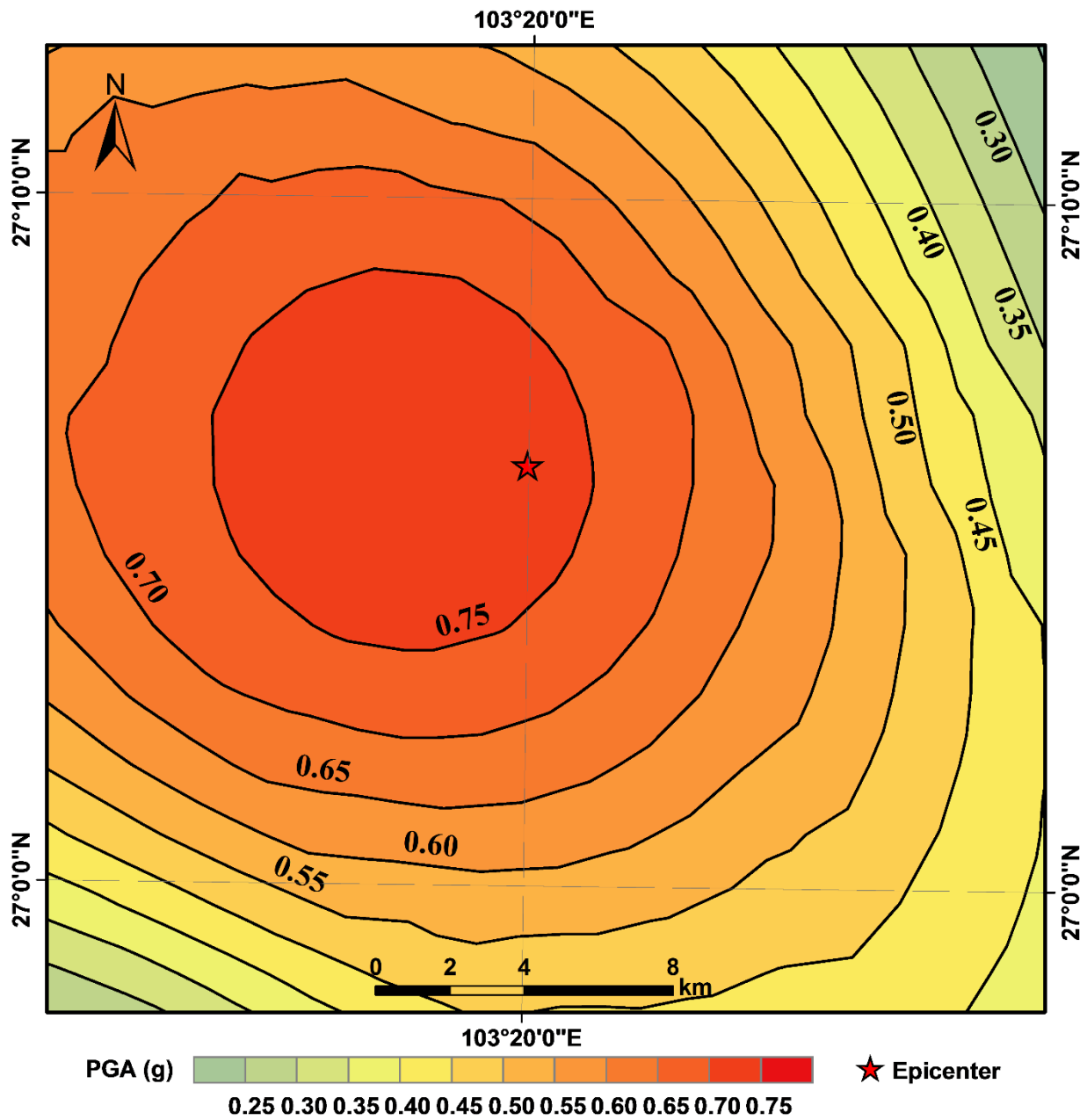
593 **Fig. 12.** Static factor-of-safety map of the study area.

594



595
 596 **Fig. 13.** Map showing critical accelerations in the study area.
 597



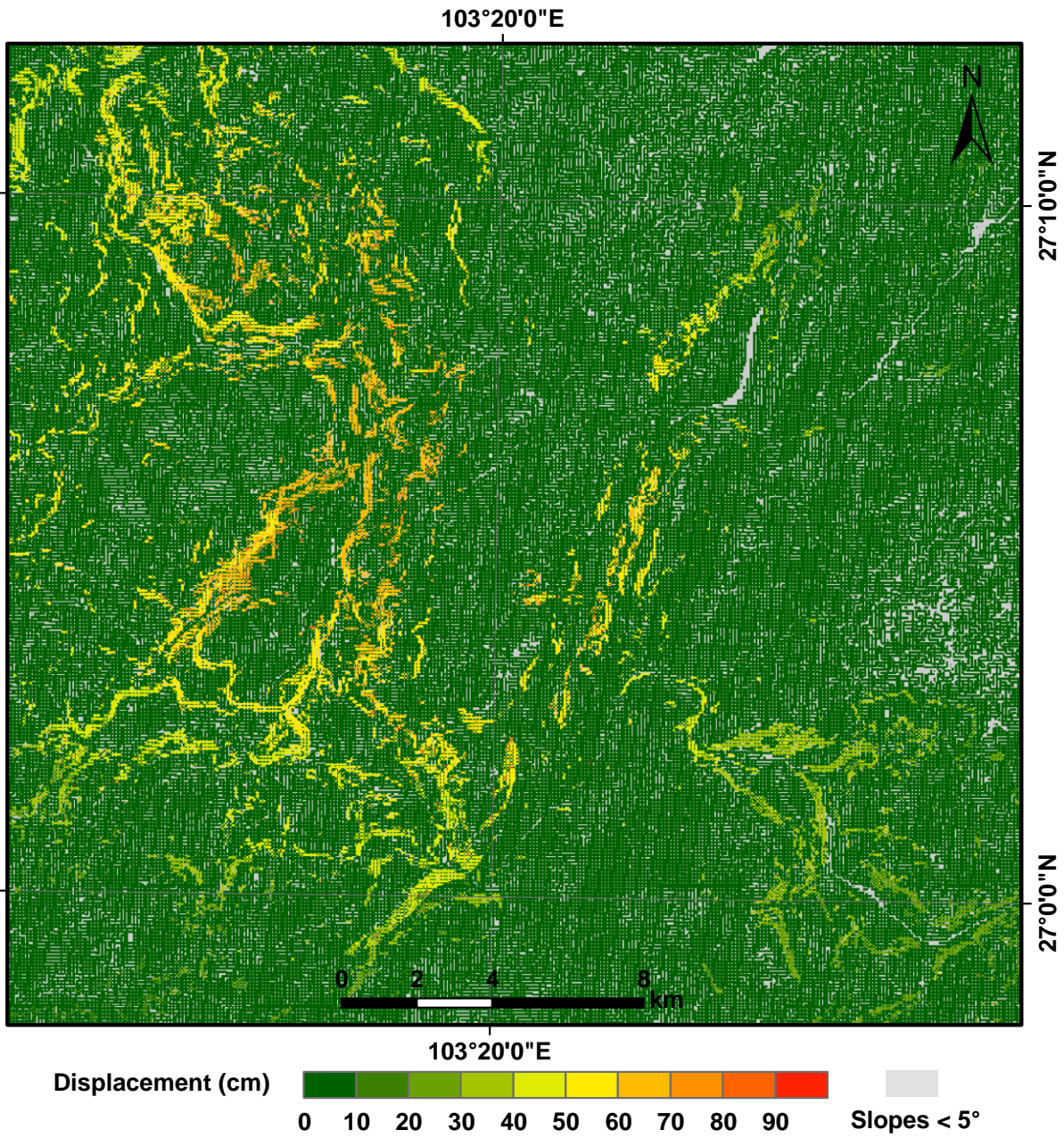


601

602 **Fig. 15.** Contour map of peak ground acceleration (*PGA*) produced by the Ludian earthquake in the

603 study area. *PGA* values shown are in *g*.

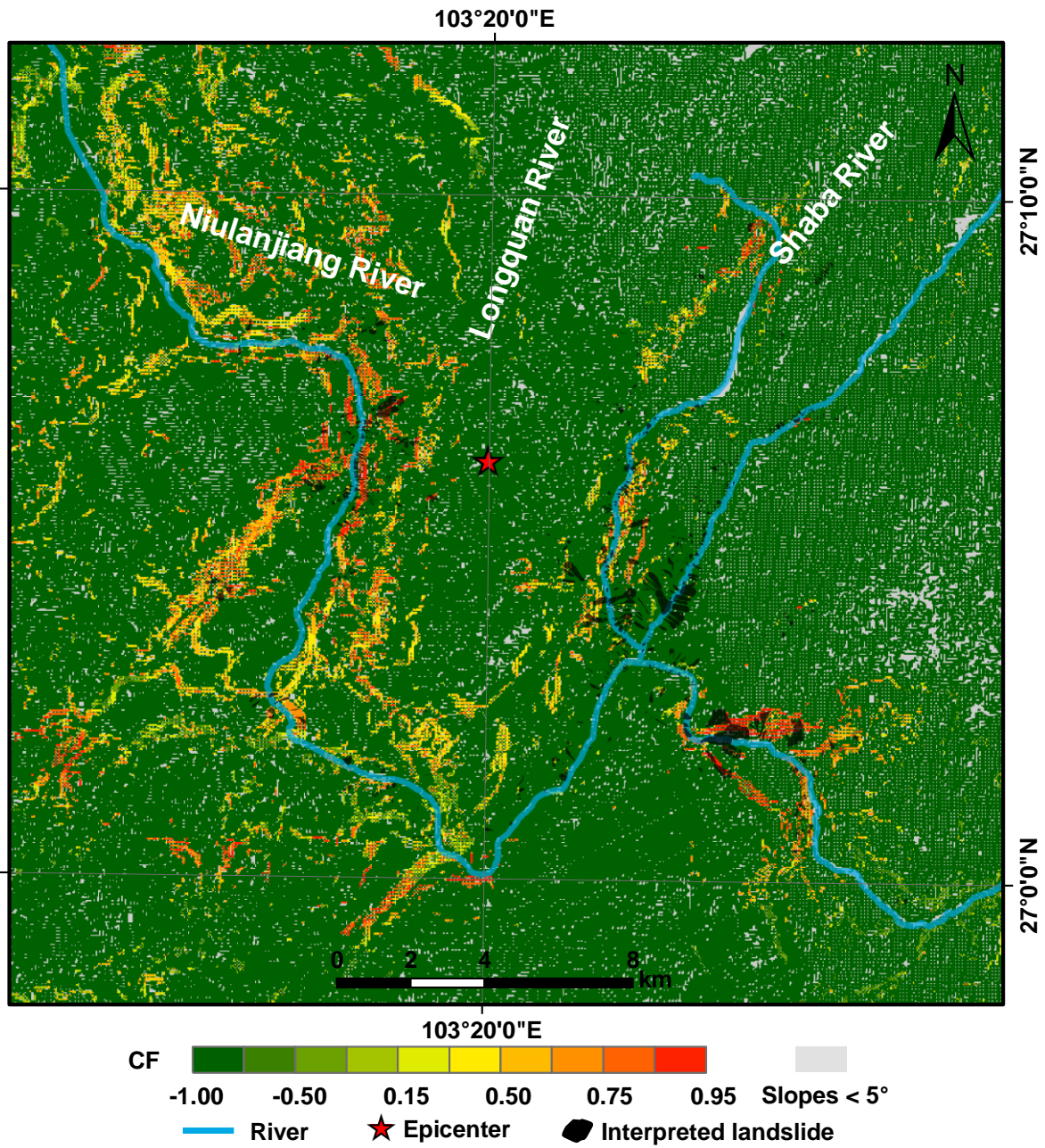
604



605

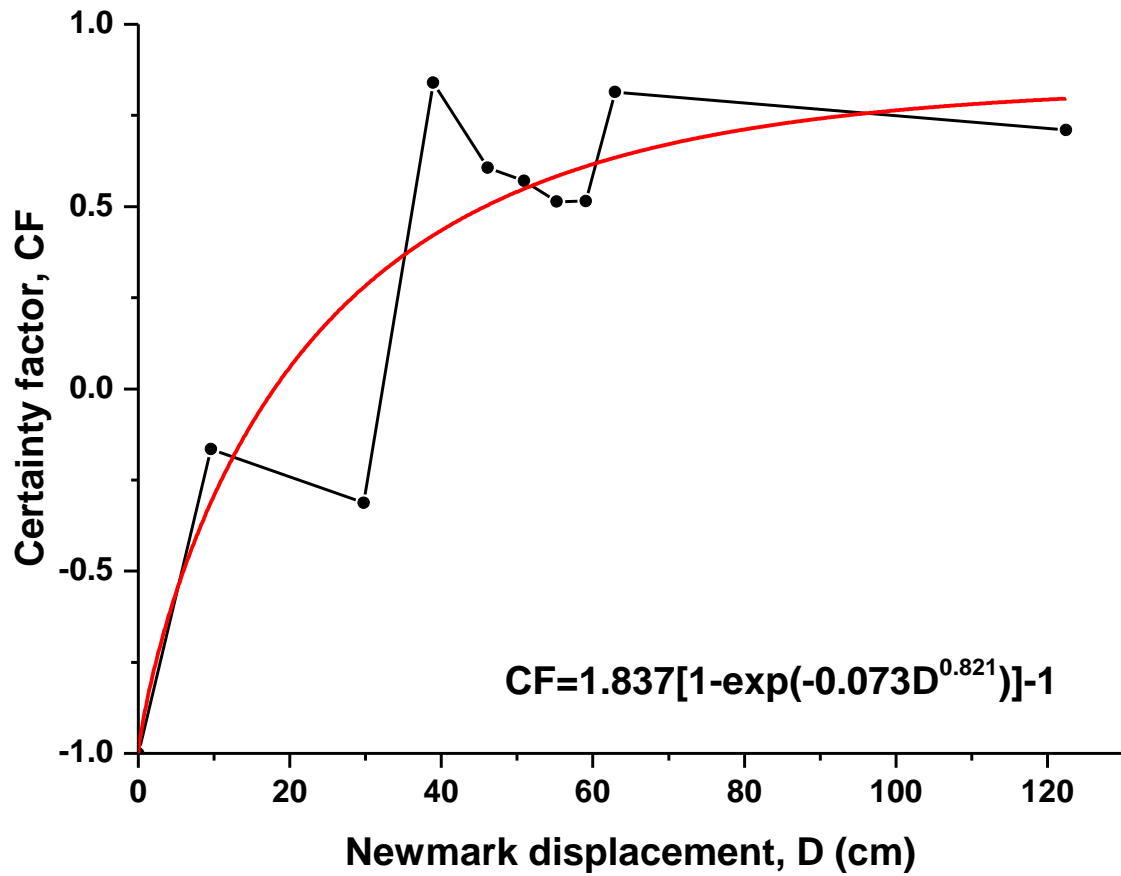
606 **Fig. 16.** Map showing predicted displacements in the study area.

607



608

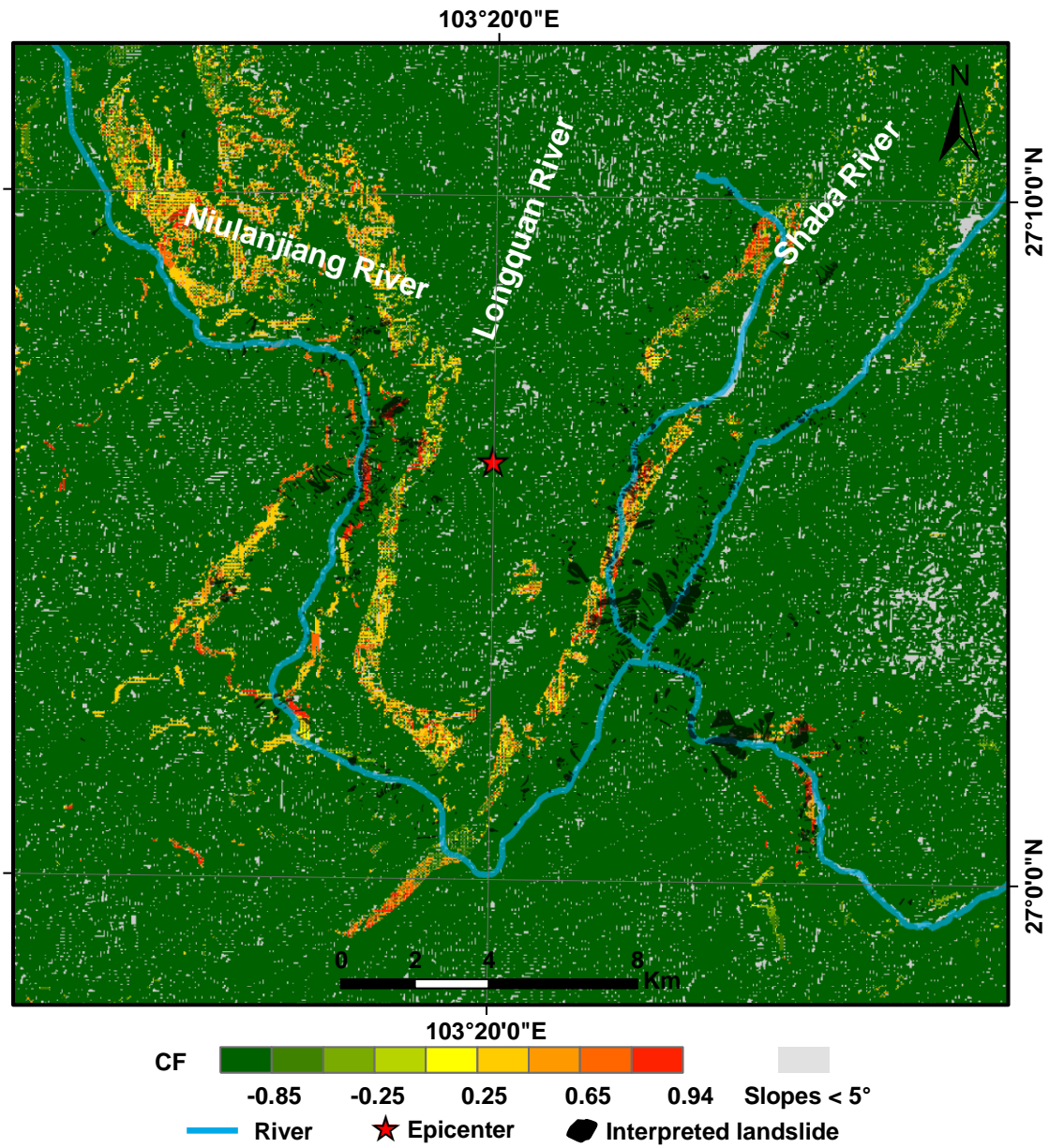
609 **Fig. 17.** Map showing confidence levels of coseismic landslides in the Ludian earthquake using **the**
 610 **proposed** method. Confidence levels are portrayed in terms of values of *CF*.



611

612 **Fig. 18.** Proportion of the area of landslides in each *CF* value area. A dot shows the *CF* value of
 613 Newmark displacement bin; the red line is the fitting curve of the data using a modified Weibull function.

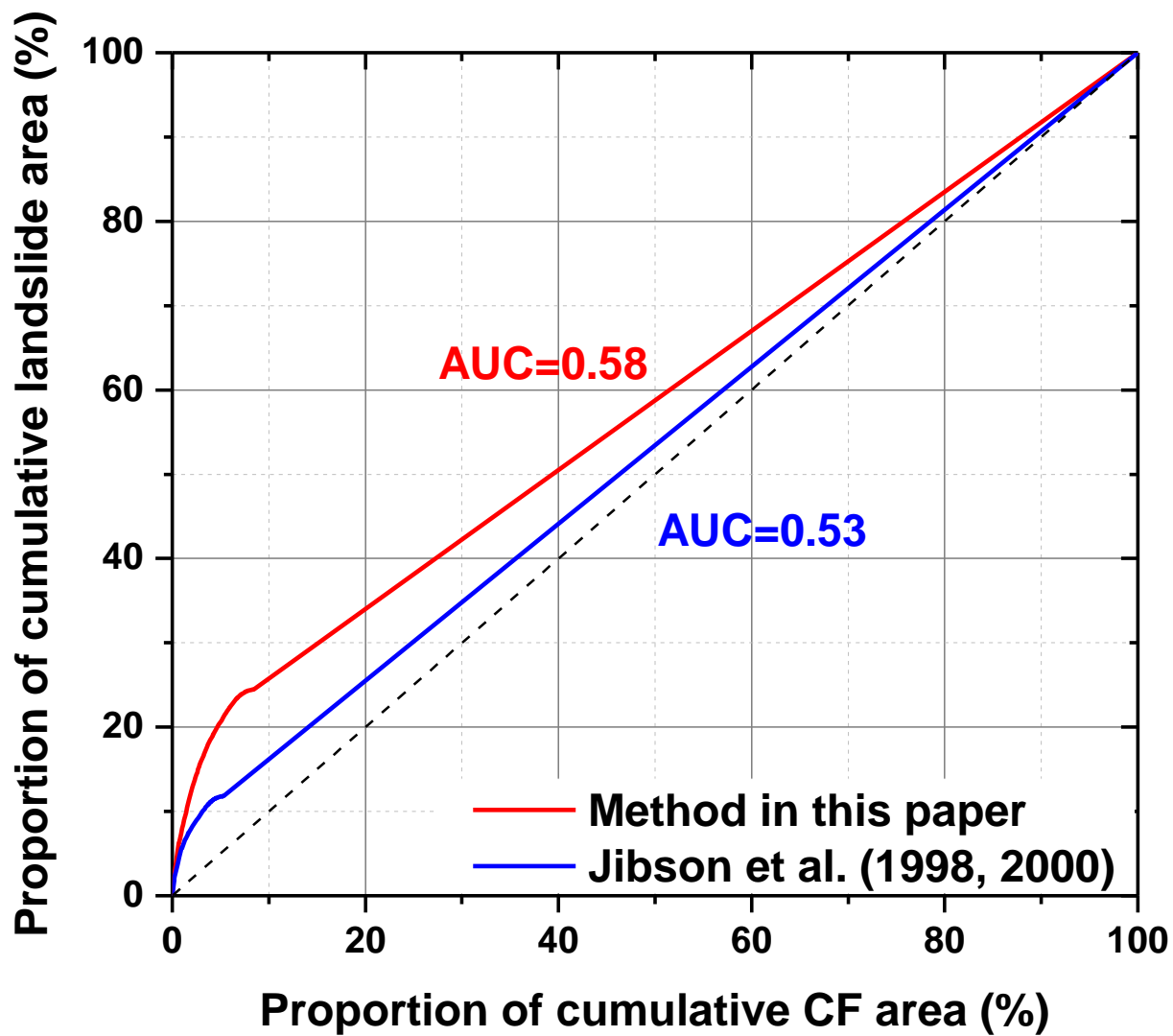
614



615

616 **Fig. 19.** Map showing confidence levels of coseismic landslides in the Ludian earthquake using a
 617 conventional Newmark analysis. Confidence levels are portrayed in terms of values of *CF*.

618



619

620 **Fig. 20.** Plots of area under the curve comparing the proposed method with the conventional Newmark's

621 method.

622

623 **Table Captions**

624 **Table 1.** Shear strengths assigned to rock types in the study area.

625 **Table 2.** Station records of three components of peak ground acceleration.

626

627 **Table 1**

628 Shear strengths assigned to rock types in the study area.

Rock type	γ (kN/m ³)	ϕ_b	JCS_0 (MPa)	JRC_0	φ	c (kPa)	References
Dolomite	25.9	32°	140	9.5	43°	35	Singh et al., 2012 Giusepone, 2014 Alejano et al., 2014 Bandis et al., 1983
Limestone	21.5	37°	160	9	45°	30	Singh et al., 2012 Yong et al., 2018 Barton and Choubey, 1977
Shale	24.9	27°	75	8	27°	16	Bilgin and Pasamehmetoglu, 1990 Coulson, 1972
Sandstone	23.5	35°	100	6	42°	24	Bandis et al., 1983 Priest, 1993 Coulson, 1972
Basalt	27.9	38°	205	8.5	50°	40	Barton and Choubey, 1977 Alejano et al., 2014 Coulson, 1972 Barton and Choubey, 1977
Slate	26.5	30°	175	3	40°	11	Bandis et al., 1983 Alejano et al., 2012 Yong et al., 2018

629 Friction angle (φ), cohesion (c), and unit weight (γ) were derived from the Geological Engineering
630 Handbook (Geological Engineering Handbook Editorial Committee, 2018)

631

No.	Station	Epicentral distance (km)	EW (g)	NS (g)	UD (g)	Average of horizontal components (g)
1	Longtoushan 1	8.114	0.5141	0.9679	0.7193	0.7410
2	Longtoushan 2	8.3	0.9685	0.7203	0.5147	0.8444
3	Qianchang	18.6	0.1490	0.1432	0.0539	0.1461
4	Ciyuan	32.6	0.0468	0.0457	0.0265	0.0463
5	Mashu	38.5	0.1380	0.1361	0.0663	0.1370
6	Qiaojia	43	0.0253	0.0210	0.0135	0.0232
7	Zhaotong 1	47.4	0.0096	0.0152	0.0065	0.0124
8	Zhaotong 2	47.671	0.0065	0.0096	0.0088	0.0081
9	Huidongxijie	63.3	0.0123	0.0128	0.0037	0.0126
10	Maolin	64.4	0.0251	0.0184	0.0111	0.0217
11	Yongshanmaolin	65.647	0.0111	0.0252	0.0184	0.0182
12	Jingan	66.2	0.0103	0.0122	0.0062	0.0113
13	Butuotuoju	66.8	0.0118	0.0173	0.0079	0.0146
14	Zhaotongjingan	67.392	0.0062	0.0103	0.0122	0.0083
15	Huidongqianxin	67.4	0.0224	0.0223	0.0067	0.0224
16	Ningnansongxin	69.2	0.0062	0.0081	0.0032	0.0071
17	Pugebaishui	76	0.0152	0.0149	0.0066	0.0151
18	Huize	76.5	0.0164	0.0182	0.0090	0.0173
19	Pugediban	81.2	0.0186	0.0127	0.0046	0.0156
20	Butuodiban	83.7	0.0024	0.0021	0.0024	0.0023
21	Tuobuka	85.2	0.0168	0.0168	0.0136	0.0168

22	Pugeyangwo	91.4	0.0066	0.0069	0.0022	0.0068
23	Daguan	91.8	0.0043	0.0035	0.0027	0.0039

634



635

636